High precision astrometry through phase-referencing VLBI at 22GHz

Towards determination of the outer Galactic rotation curve

Kazuya Hachisuka

Department of Astronomical Science
School of Mathematical and Physical Science
The Graduate University for Advanced Studies

Contents

Abstract

Feasibility of the high-precision astrometry of Galactic water maser sources was studied on the basis of fast-switching phase-referencing VLBI observations at 22GHz held with VLBA (Very Long Baseline Array) of NRAO (National Radio Astronomy Observatory) as the first step towards investigation of the structure and dynamics of the Galaxy.

Phase-referencing VLBI is a technique of observation which provides us relative position of two closely spaced astronomical radio sources with high accuracy. The technique can be applied to high-precision astrometry of Galactic maser sources using extragalactic continuum sources as reference points, yielding trigonometric parallax distances and proper motions of the maser sources throughout the Galaxy. The information obtained will be widely used in many fields of modern astronomy including, in particular, the study of the dynamics and structure of the Galaxy.

In the present observations, all ten antennas of VLBA were switched between a Galactic water maser source and an adjacent extragalactic source with a duty cycle of 40 seconds for efficient compensation of degrading effects of the atmospheric phase fluctuations. The observations of the same pair of sources were repeated twice with a month interval for detection of proper motions of the maser sources with respect to the extragalactic reference sources. Two pairs of maser and extragalactic sources were observed in this way. The observed data were reduced using the NRAO AIPS(Astronomical Image Processing System) package.

Results of observations of strong maser sources in the Galactic star forming region W3(OH) and an adjacent fairly strong extragalactic continuum source, ICRF0241+622, clearly showed that the atmospheric phase fluctuation is really well compensated though the two sources are separated by a finite angular distance of 2.17 degree. In fact, the large atmospheric phase fluctuations of several hundreds degrees observed in the fringe phases of the two sources were mostly compensated in the phase-referencing calibration

with the AIPS. After the calibration, residual error due to the atmospheric fluctuation in the resultant difference of the fringe phases averaged for a switching cycle (40 second) was about 10 degrees. The 10 degrees phase error corresponds to the positional accuracy of about 30 micro-arcseconds for a projected baseline of 2000 km, which is much better than HIPPARCOS's accuracy.

On the other hand, results of observations of another pair of Galactic and extragalactic sources : masers in Galactic star forming region IRAS21008+4700 and an adjacent extragalactic continuum source, ICRF2100+468, with angular separation of only 0.18 degree, showed about 400 micro-arcsecond displacement of the masers relative to ICRF2100+468 during a month. The displacement was almost parallel to the Galactic plane. The distance of IRAS21008+4700 is estimated to be 7.3 kpc based on the simple flat rotation model of the Galaxy. The amount and direction of the observed displacement is just consistent with the predicted proper motion of the object due mainly to the Galactic rotation and, to much lesser extent, to the Solar motion and annual parallax. Thus we conclude that we detected for the first time the proper motion due to the Galactic rotation of a distant object of several kilo-parsecs apart during only a month interval.

The proper motion was detected also for the W3(OH) and ICRF0241+622 pair. In this case, the direction of the proper motion was not parallel to the Galactic plane as expected from the proximity of W3(OH) to the Sun compared with IRAS21008+4700. In fact, at the estimated distance of W3(OH), 2.3 – 3.3 kpc , the most dominating systematic displacement comes from the annual trigonometric parallax. The predicted proper motion due to the combined effects of the annual parallax, Solar motion and Galactic rotation is fairly consistent with the observed motion. In other words, the phase-referencing VLBI observations are well capable of detecting the annual trigonometric parallaxes of Galactic sources a few kpc away.

The above results firmly show a feasibility of the phase-referencing VLBI in astrometry with high accuracy of the order of 10 micro-arcseconds. This implies that directly measured distances and proper motions of the maser

sources will be available throughout the Galaxy with the phase-referencing VLBI.

Chapter 1

Introduction and Overview

1.1 Purpose of the Present Thesis

Phase-referencing VLBI is a technique of observation which provides us relative position of two closely spaced astronomical radio sources with high accuracy. The technique can be applied to high-precision astrometry of Galactic maser sources using extragalactic continuum sources as reference points, yielding trigonometric parallax distances and proper motions of the maser sources throughout the Galaxy. The information obtained will be widely used in many fields of modern astronomy including, in particular, the Galactic dynamics (for a review, see Sofue and Rubin, 2001).

The primary purpose of the present thesis is to examine the feasibility of the high-precision measurement with the phase-referencing VLBI on the basis of real data obtained in a phase-referencing VLBI observation carried out with VLBA (Very Long Baseline Array) of National Radio Astronomy Observatory[1]. The observation was conducted as the feasibility-study step of a series of planned observations aiming at determination of the rotation curve of the Galaxy outside the solar circle.

This chapter will describe backgrounds of the present study taking into

[1]The National Radio Astronomy Observatory is operated by Associated Universities Inc., under cooperative agreement with the National Science Foundation.

account mainly recent developments in the modern astrometry and VLBI astronomy.

1.2 High precision astrometry

1.2.1 Astrometry

Astrometry is the measurement of positions, parallaxes and proper motions on the sky. It can be divided broadly into two categories: global and narrow (or small) field astrometry.

Global astrometry is concerned with mapping and cataloguing positions and motions over large areas of the sky. The measurements were traditionally based on optical telescopes, but now optical interferometers are being developed to achieve greater accuracy. A stellar reference frame of bright stars (FK5 ; ex. Fricke, 1975) has been constructed by meridian circle observations. The accuracy of all ground-based optical global astrometry is limited typically to 0.1 arcsecond level by the irregular refraction effect of the atmosphere above the telescopes, and also by thermal and mechanical instabilities in the telescopes.

Global astrometry at radio wavelengths is carried out by interferometers, with both short and very long baselines. The global astrometry with VLBI (Very Long Baseline Interferometry) uses a quantity called group delay as an observable, which is the derivative of the fringe phase with respect to frequency. Typical accuracy of the VLBI group delay astrometry reaches 1 mas (milli-arcsecond) or better (ex. Thompson et al., 1986). The VLBI group delay observations have been also applied to geodesy and proven quite successful in determining locations of the observatories on the Earth with accuracy better than 1 cm. The results of the international geodetic VLBI observations have clearly yielded present day movements of the tectonic plates or continental drifts (ex. Shaffer, 1995). However, objects of the VLBI group delay observations are exclusively the extragalactic continuum sources with minor exception of the faint Galactic continuum sources. Since the extragalacitc sources are too far to measure their parallaxes and proper

motions, the VLBI group delay astrometry has been used in limited purposes mainly related to the radio celestial reference frame, ICRF (International Celestial Reference Frame)(Johnston et al., 1995)

In narrow-field astrometry at optical, relative positions of stars are measured within the field of view observable with a long-focus telescope, by means of photographic plates or, more recently, CCDs. The relative positions are measured with greater accuracy than in the global astrometry case, because error sources including the atmospheric effects are largely common for stars observed simultaneously with a single telescope and therefore are well cancelled in the relative measurements. However, the application of the optical narrow-field astrometry has been rather limited, since relatively bright stars observable with conventional astrometry telescopes all belong to our MilkyWay Galaxy. Thus the optical narrow-field astrometry gave us relative proper motions and relative parallaxes of the Galactic stars only. Therefore, it has been mostly impossible to separately determine distance and motion of the individual stars from the data obtained by the optical narrow-field astrometry. As a consequence, the method has not been well applicable to studies of the global structure and dynamics of the Galaxy. Instead, the method has been quite powerful in discovering astrometric binaries (Benedict et al., 2000), or revealing energetic motions of the stars within a small area of the sky such as the sub parsec-scale region surrounding the Galactic center (Genzel et al., 2000).

At radio frequency, the narrow field astrometry is successfully carried out in phase-referencing (or differential) VLBI observations (ex. Beasley and Conway, 1995) to which the present thesis is addressed. The principles and methods of the observation will be described later in more detail. Here it is worthy to note that the phase-referencing VLBI can observe simultaneously or nearly simultaneously a Galactic radio source (mostly astronomical maser source) and an adjacent extragalactic radio source. In this case, we can measure absolute displacement of the Galactic source with respect to the practically immovable (except for possible movement of the relativistic jet) extragalactic source. The accuracy of the relative position measurement

could be as high as 10μas (micro-arcsecond) level, provided that the two sources are separated on the sky by no more than two degrees or so and therefore the atmospheric refraction effects are well cancelled.

1.2.2 Annual trigonometric parallax and proper motion

Measurements of the annual trigonometric parallaxes of an astronomical object provides us the most reliable way for determining distance to the object. Unlike other means for inferring cosmic distance, the trigonometric parallax measurement dose not need any assumption on the interstellar extinction, evolution of main sequence stars, motion of stellar clusters, Galactic rotation or period-luminosity relation. Unfortunately, the angular displacement due to the annual parallax is so small for most of the astronomical objects that its detection has been difficult except for stars in the immediate vicinity of the Sun (within 100 pc) in the conventional optical astrometry.

On the other hand, measurement of the proper motion of an astronomical object has been easier to conduct in the sense that the longer the interval of the repeated position measurements the larger is the angular displacement of the object during the interval due to the proper motion. Thus, the proper motion has been measured to 1 mas year^{-1} level for stars up to 1 kpc apart in the classical optical astrometry. However, the proper motion alone is not adequate to provide direct information on global parameters like Galactic rotation, Solar motion or motion perpendicular to the Galacitc plane unless we know the distance to the observed object. We cannot even convert the angular velocity of the object to the physical velocity perpendicular to the line of sight if we do not know the distance.

Therefore, it is indispensable to measure both annual trigonometric parallax and proper motion, along with the radial velocity obtainable from the spectroscopy, in order to locate the observed objects in the full six-dimensional phase space and provide a complete observational basis for the global study of the Galaxy.

1.2.3 Impact of results of HIPPARCOS mission

HIPPARCOS is an astrometry satellite launched by European Space Agency in August 1989. The satellite was in operation for more than three years and measured positions, proper motions and trigonometric parallaxes of 118,218 stars down to 12th magnitude to an accuracy of better than 1 mas. The astrometric data obtained by HIPPARCOS including very precise HR diagram of more than 15,000 field stars (Perryman et al., 1995) and determination of the distance to Hyades cluster with great accuracy (Perryman et al., 1998) provided a strong impact to the modern astronomy.

However, challenges to draw more global results on cosmology and Galactic dynamics from HIPPARCOS data suffer from difficulties due to the still limited accuracy of HIPPARCOS for those purposes. For example, the determination of the period-luminosity relation of Cephieds from HIPPARCOS data and subsequent claim on solution of the cosmological age problem by Feast et al., (1997) remain controversial (ex. Tsujimoto et al., 1998).

Therefore, the results of HIPPARCOS made us realize keenly the importance of the astrometry in the future astronomy and the needs for even higher accuracy.

1.2.4 New Projects Aiming at 10 Micro-arcsecond Astrometry

In order to achieve astrometric accuracy much superior to the one obtained by HIPPARCOS, space agencies in Europe and the United States plan to launch several astrometric satellites with optical interferometers on board.

DIVA (Double Interferometer for Visual Astrometry) is a small satellite, designed to perform astrometric and photometric observations of at least one million stars with positional accuracy of a few hundreds μas (ex. Roser et al., 1997). DIVA is planned for launch in 2004.

FAME (Full-sky Astrometric Mapping Explorer) is a small satellite designed to perform an all-sky, astrometric survey with 50 μas accuracy. FAME is a joint development effort of the US Naval Observatory and other insti-

tutions(ex. Horner et al., 1998).

SIM (Space Interferometry Mission) is being developed by the Jet Propulsion Laboratory under contract with NASA. SIM will perform astrometric measurements by comparing the fringe position of a target with the fringe positions of astrometric reference stars (or QSOs) that form an astrometric grid. Over a narrow field of view ($\leq$ 1 deg.), SIM is expected to achieve an accuracy of 1 μas. Over the maximum field of view of the instrument (10 deg.), an accuracy of better than 4 μas is expected (ex. Shao, 1998). Launch is planned in 2009.

GAIA (Global Astrometric Interferometer for Astrophysics) is the leading concept under study in the European Space Agency (ESA). This mission is to measure positions, proper motions, and parallaxes of some 50 million objects, down to about $V = 15$ mag, with an accuracy of better than 10μas, along with multi-color multi-epoch photometry of each object. (ex. Lindegren and Perryman, 1996). GAIA is expected to be launched no later than 2012.

On the other hand, the National Astronomical Observatory of Japan is promoting a phase-referencing VLBI project VERA (VLBI Exploration of Radio Astrometry) to achieve 10 μas level accuracy majorly in the astrometry of more than a thousand Galactic maser sources (ex. Honma, 2000b). All of planned four VLBI stations with the longest baseline of 2300 km are being constructed and will be completed in 2001.

1.3 Principles of VLBI

Very Long Baseline Interferometry (VLBI) is a technique in radio interferometry where telescopes, often many thousands of kilometers apart, may be operated as an interferometer to achieve great angular resolution frequently better than 1 mas. Each telescope works independently, recording the signals from a radio source on magnetic tape together with timing information. Later, the tapes are played back and the signals cross-correlated to yield scientific information reflecting the position and fine structure of the observed

source. Fundamental observables yielded by the cross-correlation processing are the fringe amplitude and the fringe phase just like in all radio interferometers. A specific feature of VLBI is the fact that it is seldom possible to get fringes automatically by means of a given set of prediction parameters on antenna locations, radio source positions and rotation model of the Earth. This is partly because of the enormously high angular resolution of VLBI compared with the possible range of errors in the predicted parameters, and more importantly because of the unpredicted effects of the atmospheric refraction over the observing stations and offsets of the independent clocks used there. Therefore, the fringes in VLBI should be searched in a process called fringe fitting. In the course of the fringe fitting two more VLBI observables are obtained : one is the fringe rate that is the derivative of the fringe phase with respect to the time and another is the group delay that is the derivative of the fringe phase with respect to the frequency as mentioned above. All these observables are used for scientific analyses of VLBI data (Thompson et al., 1986).

VLBI has achieved the highest angular resolution among all existing astronomical instruments and has been a quite powerful tool in both astronomy and geophysics. Naturally, VLBI has its own limitations however.

First, it is impossible in ordinary VLBI observations to integrate the fringe of the observed source for more than a finite duration of time called coherence time due to the irregular fluctuation of the fringe phase caused by the atmospheric refraction effects and instabilities of the independent frequency standards at observing stations. Typical VLBI coherence time is 1600 seconds at 1 GHz and as short as 16 seconds at 100 GHz (Moran 1989). This severely limits the sensitivity of VLBI. It will be discussed later that the phase-referencing VLBI is capable of overcoming the difficulty.

Second, because of the high angular resolution, VLBI is sensitive to very compact and bright sources only. To be detected by the VLBI, the angular size of a source should be of the order of the angular resolution or smaller, and the radio brightness temperature should normally $\simeq 10^6$ K or higher depending on baseline length and antenna sensitivity. Due to the

limitation, most of the thermal radio sources are not observable by VLBI. Only fairly strong nonthermal radio sources have been the targets of the VLBI observations.

Third, due to the atmospheric and instrumental phase fluctuations, it is usually impossible to fully use the fringe phase as an observable. One way to bypass the difficulty is to use the closure phase of a VLBI array in synthesis imaging (Thompson et al., 1986) and another is to use the phase-referencing VLBI as will be discussed later.

Examples of existing VLBI arrays are the Very Long Baseline Array (VLBA) in the United States (ex. Napier, 1995), the European VLBI Network (EVN) (ex. Schilizzi, 1995), the Australia Telescopes (Australian Long Baseline Array; LBA) (ex. Tzioumis,1997), Japan VLBI Network (J-Net)(ex. Omodaka, 1994) and Asia Pacific Telescope (APT) (ex. Schilizzi,1995). The advent of spaceborne radio telescopes extended VLBI baselines to hundreds of thousands of kilometers (VSOP/HALCA)(ex. Hirabayashi et al., 2000 ; Ulvestad, 1999).

The largest advantage of VLBI in astrometry over other observational techniques is its ability to relatively easily achieve high accuracy of the position measurement. In fact, the fringe spacing (or angular resolution) of a VLBI baseline, that is the angular extent of one wavelength of the interferometer fringe, is often smaller than 1 mas. For example, if we observe a radio source at frequency of 22 GHz (or at wavelength $\lambda = 1.4$ cm) with a VLBI baseline of length $D = 2000$ km, the fringe spacing is $\lambda/D \cong 1$ mas. Therefore, if we could measure the VLBI fringe phase at an accuracy level of a few degrees, we could determine a component of the radio source position in the direction perpendicular to the fringe pattern with an accuracy of 10 μas, which is much superior to that of HIPPARCOS. If we denote the signal to noise ratio of the VLBI fringe as SNR the thermal noise error in the fringe phase measurement σ_ϕ is expressed by a formula (Thompson et al., 1986),

$$\sigma_\phi = \frac{1}{SNR} \qquad \text{(radian)}. \tag{1.1}$$

Therefore, if we observe a radio source with a moderate signal to noise ratio of $SNR = 20$, then we could get the fringe phase of the source with an accuracy of about 3 degrees and hence achieve 10 μas accuracy in the position measurement, as far as the thermal noise is the only defining source of the error. Unfortunately, the unpredictable phase errors due to the irregular atmospheric refraction and instrumental instability including the clock offset are usually much larger than the thermal noise error and often exceed the VLBI fringe spacing, thus making it almost impossible to use the VLBI fringe phase as an observable for scientific analyses as mentioned above. This is the reason why the group delay and, to the lesser extent, the fringe rate have been widely used in the VLBI astrometry and geodesy, although both of them show much larger thermal noise error compared with the fringe phase.

However, the narrow-field astrometry with the phase-referencing VLBI can effectively eliminate the phase errors due to the atmosphere and the clock offset in the relative position measurements and make the difference of the fringe phases of the two adjacent radio sources a highly accurate observable for the differential astrometry.

Another advantage of the VLBI astrometry is its ability to observe both astronomical maser sources in our Galaxy and extragalactic continuum sources. Although number of the strong nonthermal sources observable with VLBI is much smaller than the number of observable objects with optical telescopes (ordinary stars), the astronomical maser sources are widely distributed throughout the whole Galaxy and the observable extragalactic sources are numerous enough that they could be normally found in the vicinity of the maser sources. Therefore, a plenty of pairs of the maser and extragalactic sources could be found for successful narrow-field astrometry (Honma et al., 2000a).

1.3.1 VLBI sources

VLBI can observe following sources:

Maser

A radio source in which the spectral lines of atoms, ions, or molecules are greatly amplified by maser (Microwave Amplification of Stimulated Emission of Radiation) action to produce an intense radio emission is called astronomical maser source. The first maser identified in space was the OH maser at 1665MHz (Weinreb et al., 1965). Maser emission is now known from many other molecules, including water (H_2O), silicon monoxide (SiO), methanol (CH_3OH), ammonia(NH_3), formaldehyde (H_2CO), hydrogen cyanide (HCN) and silicon sulphide (SiS) (Elitzur, 1992). Sometimes many spectral lines from the same molecule can be observed as masers. For example, over 30 different maser lines of SiO molecule have been observed in the circumstellar envelope of the star VY Canis Majoris. Masers usually occur in star-forming regions (interstellar masers), in the circumstellar envelopes of evolved stars in the AGB (Asymptotic Giant Branch) stage (circumstellar masers), in comets, in some planetary atmospheres, and in some active galactic nuclei (AGN) where they are so bright that they are classified as megamasers. Astronomical maser sources are usually very compact with typical size of 1 AU or smaller and exhibit very high radio brightness temperature (Reid and Moran, 1988)

AGN

The central region of a galaxy where considerable energy is generated by processes other than those operating in normal stars is called AGN (Active Galactic Nucleus). The AGNs typically show both continuum and emission-line spectra in the optical and ultraviolet bands, and frequently in the infrared, radio, and X-ray emissions. According to their radiation characteristics, the AGNs are classified into Blazers, Seyfert Galaxies and QSOs (Quasi Stellar Objects) including Quasars as their radio loud family. Radio emission from the AGNs is due mostly to the nonthermal Synchrotron mechanism. The energy source of the activity is widely explained by the accretion of material on to a black hole of up to 10^8 solar mass situated in the

very center of the galaxy. Most of the radio loud AGNs are very compact with angular size of a few mas or smaller and their brightness temperature is high. Therefore many of them are detected with the intercontinental VLBI baselines.

Others

Nonthermal radio sources in our Galaxy are also observed with VLBI. They include X-ray binaries like SS433 and Cyg X-3, relativistic-jet sources in the Galaxy like super-luminal source, nonthermal radio stars like Algol, and radio pulsars. Though they are mostly faint, VLBI observations are very important for clarifying physical nature of these interesting sources and for tying radio reference frame to the optical frame established by HIPPARCOS (Lestrade et al., 1995)

1.3.2 Achievements in VLBI Astrometry

Determinations of Distances to Maser Sources by Means of Statistical Parallax and Model-fitting Methods

Individual maser spots are extremely small, and many are clustered together in any one source. Thus, in some ways, maser sources resemble star clusters, suggesting that proper motion measurements can be used to estimate distance to them (Table 1.1).

Genzel et al (1981b) and Schneps et al (1981) measured proper motions of H_2O masers in W51(M) and W51(N), respectively. The motions in these sources appeared largely random, and the technique of statistical parallax was employed to determine distance to the sources. The distance to these sources was estimated to be 7 $\pm$ 1.5 kpc and 8.3 $\pm$ 2.3 kpc, respectively. This value is consistent with the far kinematic distance to the W51 region.

Greenhill (1993) detected proper motions of extragalactic water masers in M33. They applied the statistical parallax technique to M33, for which relative positional accuracies of about 1 μas are needed. They estimated a distance of 830 $\pm$ 250 kpc (Argon, 1998) and emphasized that this result is

Source	Method	Distance	Reference
	Galactic interstellar masers		
Orion KL	Model fitting	480 ± 80 pc	Genzel et al. (1981a)
W51 Main	Statistical parallax	7 ± 1.5 kpc	Genzel et al. (1981b)
W51 North	Statistical parallax	8.3 ± 2.5 kpc	Schneps et al. (1981)
W49 North	Model fitting	11.4 ± 1.2 kpc	Gwinn et al. (1992)
Sgr B2 North	Model fitting	7.1 ± 1.5 kpc	Reid et al. (1988a)
Sgr B2 Middle	Model fitting	6.5 ± 1.5 kpc	Reid et al. (1988b)
Cep A	Statistical parallax	500 ± 200 pc	Cawthorne et al. (1992)
W3 IRS 5	Model fitting	1.81 ± 0.10 kpc	Imai et al. (2000)
	Galactic circumstellar masers		
S Persei	Model fitting	2.3 ± 0.5 kpc	Marvel (1996)
VY Canis Majoris	Model fitting	1.4 ± 0.2 kpc	Marvel (1996)
VX Sagittarius	Model fitting	1.7 ± 0.2 kpc	Marvel (1996)
	Extragalactic masers		
M33 IC133	Statistical parallax	830 ± 250 kpc	Greenhill et al. (1993)
NGC4258	Model fitting	7.3 ± 0.4 kpc	Herrnstein et al (1997)

Table 1.1: Previous results of distance measurements with proper motions of water masers (Imai, 1999)

a preliminary distance estimate.

Although statistical parallax measurement is powerful method to determine the distance with little assumptions, this method depends on model of source kinematics.

On the other hand, model-fitting methods were made at W3 IRS 5 which is the massive star forming region with at least two different outflows (Imai et al., 2000). They performed a three dimensional kinematic model analysis of the maser motions in one of the two outflows, assuming a spherically symmetric expanding flow. They obtained a distance to the W3 IRS 5 region as 1.83 ± 0.14 kpc.

Other Studies in VLBI Maser Astronomy

VLBI maser astronomy could serve as a probe into physical conditions of maser sources, because masers emit in the dense gas in the star forming regions, circumstellar envelopes of red giant stars, molecular disks around the center of extragalaxy.

Miyoshi et al(1995) found Keplerian rotation of a molecular disk near the center of the galaxy NGC4258 (M106) by a VLBA 22GHz observation of water megamasers on the disk. This result was the decisive evidence of the presence of a massive black hole at the center of the galaxy.

It has been difficult in past studies of VLBI maser astronomy to determine positions and proper motions of maser features relative to a celestial reference point outside the maser source. The situation makes it difficult to compare emission regions of different maser lines in particular.

For example, Miyoshi et al. (1994) found in a 43GHz observation of SiO masers around AGB stars with KNIFE mm-wave VLBI that the two SiO maser lines with v=1 and v=2 emitted in the same regions around the evolved stars, and concluded on this ground that the maser lines are collisionally pumped.

However, Desmurs et al (2000), who observed AGB stars with VLBA at 43 GHz, argued that the masers are radiatively pumped because they found that the regions of emission of two lines are not generally coincident but

typically separated by 1 to 2 milli-arcseconds.

The disagreement might be solved if the locations of the regions of emission of the two lines are determined with respect to a common external reference like an extragalactic continuum source.

Phase-Referencing Astrometry

The phase-referencing VLBI observations can be divided into the simultaneous and switching observations depending if the two adjacent sources are observed simultaneously or intermittently by switching orientations of the radio telescope antennas. Here some representative results of the both types of the phase-referencing VLBI astrometry are presented (Table 1.2).

The simultaneous phase-referencing VLBI observations can be carried out most successfully when the two sources are close enough to be observed within the same antenna beam. Marcaide and Shapiro (1983) and Marcaide et al. (1994) measured relative positions of two closely spaced quasars 1038+528A and B separated by 33 arcsecond at 8.4 GHz and 2.3 GHz and achieved a very high accuracy with a statistical error as small as several μas.

Fomalont et al (1999) measured parallaxes and proper motions of two pulsars B0919+06 and B1857-26 with respect to extragalactic sources found in their very vicinity. Parallaxes obtained for the two pulsars were 0.31±0.14 mas and 0.5±0.6 mas, respectively. Sawada-Satoh et al (2000) detected weak continuum sources in the center of a Seyfert 2 galaxy NGC3079 by phase-referencing to strong water maser sources observed in the same circumnuclear region of the galaxy and succeeded to distinguish a central core and jet components by measuring their proper motions with respect to the masers.

When the angular separation of the two sources exceed the antenna beam size, multiple telescopes in each VLBI station can be used to track different sources simultaneously (Counselman et al., 1974; Rioja et al., 1997). Japanese project VERA will use a new steerable dual-beam receiving system in orde to facilitate simultaneous tracking of two adjacent sources with a single Cassegrain antenna.

The switching phase-referencing VLBI observations have been used more widely than the simultaneous observations since the method allowed to realize relatively easily the phase-referencing observations for source pairs with finite angular separations with existing radio telescope antennas, though naturally the compensation of the atmospheric phase fluctuation is not as effective as in the simultaneous case.

Gwinn et al. (1986) carried out switching phase-referencing VLBI between pulsars and adjacent quasars at 1.66 GHz with switching cycle of 4 to 7 minutes. For pulsars PSR0823+16 and PSR0950+08, they obtained parallaxes of 2.8±0.6 and 7.9±0.8 mas, respectively. Bartel et al. (1986) observed quasar 3C345 and an adjacent more distant compact quasar NRAO512 at 2.3 and 8.4 GHz with switching cycle of 3 to 7 minutes. They set an upper limit for the motion of the core of 3C345 with respect to NRAO512 to be 12±8 μas year^{-1} for right ascension and 28±21 μas year^{-1} for declination, thus showing that the core is practically at rest compared with jet components of 3C345 which exhibit much larger superluminal motions. Reid et al. (1999) detected 5.90±0.4 mas year^{-1} proper motion of Sgr A*, the compact radio source at the Galactic center, relative to adjacent extragalactic radio sources in a series of 43GHz phase-referencing VLBI observations with switching cycle of 30 sec. Due to the low elevation of Sgr A* at VLBA sites and the high observing frequency (43GHz), the fluctuation of the fringe phase was large and they suffered from difficulty in connecting 360° jumps of the fringe phase. As a result, they have not succeeded yet to detect the annual parallax of Sgr A*. Ros (1999) determined angular separations of three adjacent radio sources, BL Lac objects 1803+784 and 2007+777 and the quasar 1928+738 forming a triangle, with the phase-referencing technique at 2.3 and 8.4 GHz and with switching cycle of 9 minutes (2 minutes on source and 1 minute for slewing). They successfully connected differenced phase at 7° level at 8.4 GHz. The accuracy of the determination of the angular separations was about 0.1 mas. Guirado Guirado et al. (2000) demonstrated the feasibility of phase-referencing VLBI observation at millimeter wavelength, λ = 7 mm. They determined angular separation of

BL2007+777 and QSO1928+738 with the order of tens micro arcseconds accuracy. Moreover, the separation angle between these sources were 4.6 degrees, then this result showed the possibility of extragalactic dynamics directly at high frequency. Pérez-Torres et al. (2000)et al. demonstrated the feasibility of phase-referencing VLBI astrometry over 15° on the sky. They determined angular separation of QSO1150+812 and BL1803+784 at 8.4 and 2.3 GHz with an accuracy of better than 1 milli-arcsecond. This result opens the avenue for the application of phase-referencing VLBI technique on a full-sky scale.

Lestrade et al (1999) carried out multi-epoch phase-referencing VLBI observations of 11 radio-emitting stars which have been conducted as part of an astrometric program to link the HIPPARCOS optical reference frame to the radio extragalacitc reference frame. The mean astrometric precision achieved relative to the reference source is 0.36 mas. They presented the VLBI positions, proper motions and trigonometric parallaxes with this precision.

Sjouwerman et al (1998) attempted to measure positions of SiO maser sources located near the Galactic center relative to Sgr A* at 43 GHz with switching cycle of 40 seconds. Because of the large atmospheric phase fluctuation at 43 GHz and limitation in sensitivity, they could detect only 2 sources out of 10. The results showed difficulties of switching phase-referencing VLBI at high frequency and at low elevation. van Langevelde et al(2000) measured annual parallax of an OH maser source located on an evolved star U Her with respect to adjacent extragalacitc continuum sources at 1.6 GHz. The maser source and the reference extragalactic sources were observed every 5 to 7 minutes. The absolute radio position of the maser was consistent with the stellar optical position measured by HIPPARCOS at the accuracy level of 15 mas.

Target source	Reference source	Frequency (GHz)	Separation angle	Switching cycle	Reference
Galactic sources as a target source					
PSR0823+16	0822+272	1.7	0.51 deg.	4 - 7 min.	Gwinn et al. (1986)
PSR0950+08	0938+119	1.7	4.8 deg.	4 - 7 min.	Gwinn et al. (1986)
OH/IR stars (SiO masers)	Sgr A*	43	4.8, 8.4 arcmin.	40 sec.	Sjouwerman et al. (1998)
Sgr A*	J1745-283	43	1.3 deg.	30 sec.	Reid et al. (1999)
B0919+06	J0923+0638	1.5	12 arcmin.	—	Formalont et al. (1999)
B1857-26	J1900-2602	1.5	7 arcmin.	—	Formalont et al. (1999)
star (binary)	adjacent extragalactic sources	5.0, 8.4	0.5 - 4.5 deg.	5 min.	Lestrade et al. (1999)
U Her (OH masers)	1628+214, 1636+2112	1.7	2.8, 3.4 deg.	5.5 min.	van Langevelde et al. (2000)
IRAS21008+4700 (H_2O masers)	**2100+468**	**22**	**0.18 deg.**	**40 sec.**	**Present work**
W3(OH) (H_2O masers)	**0241+622**	**22**	**2.17 deg.**	**40 sec.**	**Present work**
Extragalactic sources as a target source					
1038+582A	1038+582B	8.4, 2.3	33 arcsec	—	Marcaide and Shapiro (1984)
NRAO512	3C345	2.3, 7.9, 8.4, 10.7	0.48 deg.	4-7 min.	Bartel et al. (1986)
1803+784,2007+777,1928+738		2.3, 8.4	6.4, 4.6, 6.8 deg.	9 min.	Ros et al. (1999)
1928+738	2007+777	43	4.6 deg.	110 - 300 sec.	Guirado et al. (2000)
1803+784	1150+812	2.3, 8.4	15 deg.	7 min.	Pérez-Torres et al. (2000)
NGC3079 (H_2O masers)	NGC3079 (continuum)	22	7 mas	—	Sawada-Satoh et al. (2000)

Table 1.2: Previous and present outlines of the phase-referencing VLBI astrometric observation. In column of switching cycle, the symbol "—" means the "in-beam style" observation.

1.4 Why were Galactic water maser sources selected?

As stated earlier, the present thesis is addressed to the study of the feasibility of the high-precision astrometry of Galactic H_2O masers with the phase-referencing VLBI. Generally speaking, all bright maser sources, including OH, SiO and H_2O masers, could be targets of Galactic astrometry, since they are all well observed with VLBI and associated with young and evolved stars widely distributed throughout the Galaxy. However, we selected only H_2O masers in the present study on the following grounds.

1. For OH masers at 1.6 GHz, the fringe spacing is 13.8 times as large as the one for H_2O masers if the two masers are observed on the same baseline. Consequently, the astrometric accuracy gets 13.8 times lower if the phase errors for both of the masers are the same. We need in particular much higher signal-to-noise ratio in OH maser astrometry than in H_2O maser astrometry, in order to suppress the thermal noise error to the same level.

2. On the other hand, compensation of the atmospheric phase fluctuation is more difficult for SiO masers at 43 GHz than for H_2O masers at 22 GHz, since the same excess-path fluctuation causes almost twice as large phase fluctuation at 43 GHz than at 22 GHz. The phase fluctuation caused severe difficulty in 43 GHz switching phase-referencing VLBI in the direction of the Galactic center (Reid et al., 1999; Sjouwerman et al., 1998).

3. A simulation of the tropospheric phase fluctuation effect in a switching phase-referencing VLBI observation was conducted based on a model, which assumes Kolmogorov turbulence, frozen flow and a phase screen with realistic parameters on the fluctuating propagation delay (Sasao, 1997). The similar simulation was proven useful in phase compensation experiments conducted with Nobeyama Millmeter Array (Asaki et al., 1996). The simulation results showed that the phase-referencing

observation will be successful and RMS time-averaged fluctuation of the differential excess path length after an hour of the phase-referenced integration will be smaller than 0.1mm (10 μas for 2000km projected baseline), provided that the switching cycle is shorter than 40 seconds, the sources are separated by less than 2 degrees and observing frequency is around 22 GHz.

4. Moreover, phase-referencing VLBI observation of H_2O maser and extragalactic sources has not been made yet. Therefore, it is important to show the feasibility of this kind of observation for the first time and to open a prospect towards the high-precision Galactic astrometry.

1.5 Thesis Overview

Principles of phase-referencing VLBI observation are described in Section 2. Section 3 describes present phase-referencing VLBA observation at 22 GHz. Reduction procedure of the observed data with AIPS is described in Section 4. Results of VLBA observations are presented in Section 5. Section 6 examines various sources of errors affecting the phase-referencing astrometric observations. In section 7, implications of the obtained displacements of the maser positions during a month and feasibility of the high-precision phase referencing VLBI astrometry are discussed.

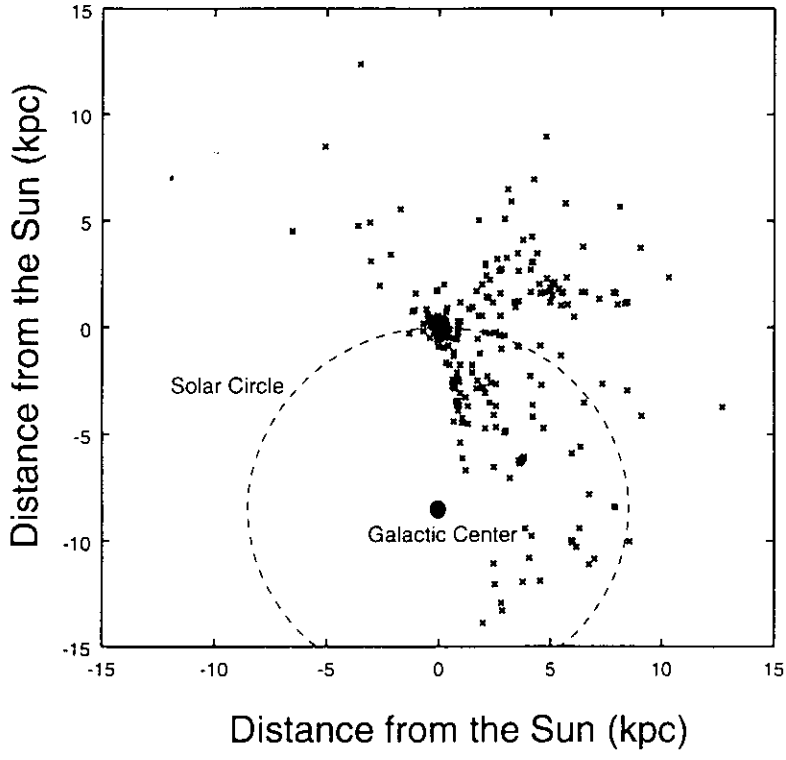

Figure 1.1: Distribution of water maser sources in the Galaxy. These water maser sources were selected from Arcetri catalog (ex. Palagi et al. 1993). These sources are distributed throughout the Galaxy, then, they are useful for study of the dynamics and structure of the Galaxy.

Chapter 2

Principles of the Phase-referencing VLBI

2.1 Fringe Phase in VLBI Observations

The cross-correlation $r(t)$ of radio signals received at two antennas of a two-element interferometer generally shows a quasi-sinusoidal time behavior, called fringe, which is expressed, when the radio signal is approximated by a monochromatic wave, by the form

$$r(t) = A \cos \phi_I, \tag{2.1}$$

where A and ϕ_I are the amplitude and phase, respectively, of the fringe pattern widely referred to as fringe amplitude and fringe phase. The fringe amplitude depends on the flux density and the structure of the observed source, the gain characteristics of the antennas and receivers, and the attenuation of the radio wave in the propagation media. The major component ϕ_g of the fringe phase ϕ_I in equation (2.1) comes from the geometrical path-length difference of the radio signal reaching to each of the two antennas:

$$\phi_{\rm g} = 2\pi\nu \left(\frac{\mathbf{D} \cdot \mathbf{s}}{c} \right) \equiv 2\pi\nu\tau_g, \tag{2.2}$$

where $\mathbf{D}$ is the baseline vector between the two antennas, $\mathbf{s}$ is a unit vector towards the brightness center of the observed source, c is the speed of light,

ν is the observing frequency, and $\tau_{\rm g}$ is the geometrical delay that is the difference in arrival times of the same wavefront from the observed source at the two antennas. The geometrical delay $\tau_{\rm g}$ and hence the phase component $\phi_{\rm g}$ is a function of the direction of the incoming radio wave with respect to the baseline and in general changes rapidly with the diurnal motion of the Earth. The total fringe phase ϕ_I includes also difference of instrumental phase errors in the two antenna systems, the visibility phase reflecting the structure (brightness distribution) of the observed source and, in case of VLBI, the excess phase due to the difference in propagation delays caused by the refraction in the atmosphere and offset of the independent clocks at the two stations.

In the course of the cross-correlation processing of interferometric data, a predicted phase, which is calculated by equation (2.2) with adopted models of the antenna locations and the source position, is corrected from the observed fringe phase. The residual VLBI fringe phase ϕ after the correction is now expressed as

$$\begin{aligned} \phi(t) &= \Delta\phi_{\rm g}(t) + \phi_{\rm stru}(t) + \phi_{\rm atmo} + \phi_{\rm inst}(t) \\ &\quad +(\text{thermal noise}), \end{aligned} \tag{2.3}$$

where $\Delta\phi_{\rm g}$ is the residual phase error due to geometric errors in the delay model, $\phi_{\rm stru}$ is the visibility phase due to the source structure, $\phi_{\rm atmo}$ is the phase error due to the propagation delays caused by the refraction in the atmospheric layers above the antennas, and $\phi_{\rm inst}$ is any instrumental phase error including the one due to the clock offset.

The term $\Delta\phi_{\rm g}$ is given by

$$\begin{aligned} \Delta\phi_{\rm g} &= 2\pi\nu\frac{\Delta\left(\mathbf{D}\cdot\mathbf{s}\right)}{c} \\ &\equiv 2\pi\nu\left(\frac{\mathbf{D}\cdot\mathbf{s}}{c}\right)_{\rm obs} - 2\pi\nu\left(\frac{\mathbf{D}\cdot\mathbf{s}}{c}\right)_{\rm model}. \end{aligned} \tag{2.4}$$

The geometric phase errors in the delay model can be separated into

errors due to source positions and antenna positions. Then, $\Delta(\mathbf{D}\cdot\mathbf{s})$ can be written as

$$\Delta(\mathbf{D}\cdot\mathbf{s}) = \mathbf{D}_0\cdot\Delta\mathbf{s} + \Delta\mathbf{D}\cdot\mathbf{s}_0, \tag{2.5}$$

where subscript 0 means adopted quantities in the correlator model, $\Delta\mathbf{D}$ is the residual baseline length due to the uncertainty in the adopted antenna locations, and $\Delta\mathbf{s}$ is the offset of source positions relative to a reference point.

The term ϕ_{stru} can be written as

$$\phi_{stru} = \arg\left[\iint I(x,y)e^{-i2\pi(ux+vy)}\,dx\,dy\right], \tag{2.6}$$

where I is the brightness distribution of radio source in the sky and u, v are projected baseline components normalized by the wavelength.

As mentioned in the previous chapter,

$$\phi_{\mathrm{atmo}} = 2\pi\nu\tau_{\mathrm{atmo}}, \tag{2.7}$$

where τ_{atmo} is the propagation delay due to the atmospheric refraction effect and

$$\phi_{\mathrm{inst}} = 2\pi\nu\left(\tau_{\mathrm{clock}} + \tau_{\mathrm{cable}}\right) + \tau_{\mathrm{local}}, \tag{2.8}$$

where τ_{clock} is the clock offset, τ_{cable} is delay in the receivers and transmission system, and τ_{local} is the phase error in the local oscillator, are usually large and unpredictable in the VLBI observations. Especially, the atmospheric term ϕ_{atmo} shows highly irregular and fairly large time variation often exceeding 360° due mainly to the water vapor component in the turbulent troposphere. The large unpredictable phase errors make it practically impossible to use the fringe phase in the most of the analyses of the ordinary VLBI observations.

It is the common practice in the VLBI imaging to use the closure phase, when the observing VLBI array consists of more than three stations, in order to eliminate all unnecessary phase terms due to the atmospheric and

instrumental effects while keeping the large part of the information on the visibility phase $\phi_{\rm stru}$. In the closure-phase method, however, the information on the absolute position of the source brightness center is totally lost.

Another way to correct for the atmospheric and instrumental phase errors in the VLBI imaging is the so-called self-calibration method where the fringe phase of a bright compact spot (if any) in the source structure is used to calibrate the phase of the other part of the source image map. This is a kind of the phase-referencing within a single source which allows us to recover a sharp image of the source structure without affected by the atmospheric and instrumental phase errors. But again the information on the absolute position of the source is missed in this method.

2.2 Phase-difference in the Phase-referencing VLBI

As described in the previous chapter, the target source of our interest is observed with an adjacent reference source simultaneously or nearly simultaneously (by switching antenna directions) in the phase-referencing VLBI observations.

Since the analysis in the present thesis is made for the observations carried out in the switching mode using the VLBA array, we describe here how the atmospheric and instrumental phase errors are calibrated in the case of the switching phase-referencing VLBI observations.

Assuming that the reference source is observed at time t_1, the measured residual fringe phase $\phi_{\rm ref}(t_1)$ for the reference source is from equation (2.3) and (2.5)

$$\begin{aligned}\phi^{\rm ref} &= 2\pi\nu\frac{\mathbf{D}_0^{\rm ref}(t_1)\cdot\Delta\mathbf{s}^{\rm ref}(t_1)}{c}+2\pi\nu\frac{\Delta\mathbf{D}^{\rm ref}(t_1)\cdot\mathbf{s}_0^{\rm ref}(t_1)}{c}+\phi_{\rm stru}^{\rm ref}(t_1)\\ &\quad+\phi_{\rm atom}^{\rm ref}(t_1)+\phi_{\rm inst}^{\rm ref}(t_1)+\text{thermal noise}^{\rm ref},\end{aligned}\tag{2.9}$$

where notations are similar to those in equation (2.3) and (2.5).

Let the target source be observed at time t_2 after a quick slewing of antennas. Then the measured residual fringe phase for the target source

$\phi_{\rm targ}(t_2)$ is

$$\begin{aligned}\phi^{\rm targ} &= 2\pi\nu\frac{\mathbf{D}_0^{\rm targ}(t_2)\cdot\Delta\mathbf{s}^{\rm targ}(t_2)}{c}+2\pi\nu\frac{\Delta\mathbf{D}^{\rm targ}(t_2)\cdot\mathbf{s}_0^{\rm targ}(t_2)}{c}+\phi_{\rm stru}^{\rm targ}(t_2)\\ &\quad+\phi_{\rm atom}^{\rm targ}(t_2)+\phi_{\rm inst}^{\rm targ}(t_2)+\text{thermal noise}^{\rm targ}. \qquad (2.10)\end{aligned}$$

where again notations are much the same as in equation (2.3).

Then, the reference source is observed again at time t_3 and the target source at time t_4, and so on.

After adjusting the epochs of the residual fringe phase time series of the reference and target sources to common epochs by a suitable interpolation, their difference is formed as

$$\begin{aligned}\phi^{\rm targ}-\phi^{\rm ref} &= \left(2\pi\nu\frac{\mathbf{D}_0^{\rm targ}\cdot\Delta\mathbf{s}^{\rm targ}}{c}+2\pi\nu\frac{\Delta\mathbf{D}^{\rm targ}\cdot\mathbf{s}_0^{\rm targ}}{c}+\phi_{\rm stru}^{\rm targ}\right)\\ &\quad-\left(2\pi\nu\frac{\mathbf{D}_0^{\rm ref}\cdot\Delta\mathbf{s}^{\rm ref}}{c}+2\pi\nu\frac{\Delta\mathbf{D}^{\rm ref}\cdot\mathbf{s}_0^{\rm ref}}{c}+\phi_{\rm stru}^{\rm ref}\right)\\ &\quad+\left(\phi_{\rm atmo}^{\rm targ}-\phi_{\rm atmo}^{\rm ref}\right)+\left(\phi_{\rm inst}^{\rm targ}-\phi_{\rm inst}^{\rm ref}\right)\\ &\quad+(\text{thermal noise})^{\rm targ}+(\text{thermal noise})^{\rm ref}. \qquad (2.11)\end{aligned}$$

Now the following reasonable approximations can be made at this point.

- $\phi_{\rm atmo}^{\rm targ}\cong\phi_{\rm atmo}^{\rm ref}$:
  the reference and target sources are close enough on the sky that the atmospheric phase errors are almost the same along the lines of sight towards the sources.
- $\phi_{\rm inst}^{\rm targ}\cong\phi_{\rm inst}^{\rm ref}$:
  the instrumental phase errors should be much the same for the reference and target sources during the one cycle of the fast switching.
- $\mathbf{D}_0^{\rm targ}=\mathbf{D}_0^{\rm ref}=\mathbf{D}_0$ and $\Delta\mathbf{D}^{\rm targ}=\Delta\mathbf{D}^{\rm ref}=\Delta\mathbf{D}$:
  since the same antennas are used for the target and reference sources.

In addition, if the reference and target sources both have very compact or simple symmetrical structures, we can further assume that $\phi_{\rm stru}^{\rm targ} \cong 0$ and $\phi_{\rm stru}^{\rm ref} \cong 0$. Moreover, if the separation angle is very small between reference and target sources or the adopted antenna location is consistent with true location, we can assume that $\Delta\mathbf{D} \cdot \left(\mathbf{s}_0^{\rm targ} - \mathbf{s}_0^{\rm ref}\right) \cong 0$.

Then, the differential phase $\Delta\phi$ is reduced to

$$\begin{aligned} \phi^{\rm targ} - \phi^{\rm ref} &= 2\pi\nu \frac{\mathbf{D}_0 \left(\cdot\Delta\mathbf{s}^{\rm targ} - \Delta\mathbf{s}^{\rm ref}\right)}{c} \\ &\quad + (\text{thermal noise})^{\rm targ} + (\text{thermal noise})^{\rm ref} \end{aligned} \tag{2.12}$$

Thus the differential fringe phase now contains only the information about the position of the target source relative to the reference source, $\Delta\mathbf{s}^{\rm targ} - \Delta\mathbf{s}^{\rm ref}$. Since the most degrading effects of the atmospheric phase fluctuation and the instrumental phase error are largely eliminated, the differential phase can be measured with a high accuracy nearly at the level of the small thermal noise error. Therefore, the differential phase offers a great possibility for the highly precise differential astrometry.

In the actual data reduction process described below, the adjustment of the time epoches of the two data series for the reference and target sources and formation of the difference of the residual fringe phases are performed by applying the calibration table for the reference source to the target source with a series of tasks in the NRAO AIPS (Astronomical Image Processing System) package.

Chapter 3

Observation

3.1 Very Long Baseline Array

The Very Long Baseline Array (VLBA) of NRAO (National Radio Astronomy Observatory) is a highly flexible VLBI Array designed for wide fields of research in high resolution astronomy and geodesy. The VLBA has ten stations spread over the whole United States of America, from Hawaii to Caribbean Sea (Table 3.1). Aperture diameter of each antenna is 25 m. Each antenna is equipped with receivers for 8 bands for two polarizations which cover the frequency range from 300 MHz to 43 GHz. The VLBI backend used is called 'VLBA Terminal' with the maximum recording speed of 256 Mbps.

3.2 Observed Radio Sources

Since the purpose of the VLBI observations discussed in the present thesis is to show the feasibility of the high-precision measurement of positions of the astronomical maser sources with respect to adjacent extragalactic continuum sources, two typical pairs of water maser and extragalactic sources IRAS21008+4700 - ICRF2100+468 and W3(OH) - ICRF0241+622 were selected and observed at 22GHz frequency band (table 3.2).

	SC	HN	NL	FD	LA	PT	KP	OV	BR	MK
Sainte Croix (SC)		2853	3645	4143	4458	4579	4839	5460	5767	8611
Hancock (HN)	2853		1611	3105	3006	3226	3623	3885	3657	7502
North Liberty (NL)	3645	1611		1654	1432	1663	2075	2328	2300	6156
Fort Davis (FD)	4143	3105	1654		608	564	744	1508	2345	5134
Los Alamos (LA)	4458	3006	1432	608		236	652	1088	1757	4970
Pietown (PT)	4579	3226	1663	564	236		417	973	1806	4795
Kitt Peak (KP)	4839	3623	2075	744	652	417		845	1913	4466
Owens Valley (OV)	5460	3885	2328	1508	1088	973	845		1214	4015
Brewster (BR)	5767	3657	2300	2345	1757	1806	1913	1214		4398
Mauna Kea (MK)	8611	7502	6156	5134	4970	4795	4466	4015	4398	

Table 3.1: VLBA baseline lenghts in km

Water masers in a star forming region IRAS21008+4700 are relatively faint with flux density of 40 Jy according to the Arcetri H_2O Maser Catalog (Cesaroni et al. 1988, Comoretto et al. 1990, Palagi et al. 1993 and Brand et al. 1994). The flux density is just sufficient to be detected with the VLBA sensitivity. Though faint, the maser source has a suitable reference source ICRF2100+468 at a very small angular distance of 0.18 degrees (table 3.6).

ICRF2100+468 is known as a variable source in the Galactic plane at radio and infrared frequency bands (Gregory and Taylor 1981, Norton et al, 1993). ICRF2100+468 is an unresolved (< 0.1 arcsec) point source with VLA (Duric et al, 1987). HI data suggest that ICRF2100+468 is an extragalactic source (Taylor and Seaquist 1984). However, Elias et al. (1985) reported that their infrared observations are not sufficient to distinguish if ICRF2100+468 is a Galactic or extragalactic object.

On the other hand, angular separation between W3(OH) and ICRF0241+622 is relatively large (2.17 degrees as listed in table 3.6). But water masers in W3(OH) are very strong with flux density up to 4000 Jy according to the Arcetri Catalog. The reference source ICRF0241+622 is also fairly bright (1.25 Jy at 22 GHz according to VLA Calibrator Manual). Its redshift is equal to 0.044 (Hewitt and Burbidge,1987), which corresponds to a distance of 175 Mpc ($H_0 = 75$km s^{-1} Mpc^{-1}).

Table 3.2: Observed sources

Target source	Reference source	Calibrator
IRAS21008+4700	ICRF2100+468	3C454.3
W3(OH)	ICRF0241+622	NRAO150

Table 3.3: Source coordinates in J2000

	Right ascension H M S	Declination D M S	Gal. Longitude degree	Gal. Latitude degree
IRAS21008+4700	21:02:33.01	+47:12:26.2	88.8	0.74
ICRF2100+468	21:02:17.057	+47:02:16.25	—	—
W3(OH)	02:27:04.83	+61:52:24.607	134.7	1.07
ICRF0241+622	02:44:57.697	+62:28:06.52	—	—

Therefore, the W3(OH)-ICRF0241+622 pair could be used to examine how well the atmospheric phase fluctuation can be compensated in the phase-referencing VLBI when the sources are separated by a finite angular distance as large as two degrees. On the other hand, IRAS21008+4700 - ICRF2100+468 pair is appropriate to see how precisely the position of the relatively faint source can be measured when the atmospheric phase fluctuation is well compensated.

The reference sources are selected from the ICRF (International Celestial Reference Frame) Catalog (Johnston et al, 1995) where the most frequently observed compact continuum sources with precisely determined celestial positions are listed and used in the world geodetic VLBI observations.

The source pairs are selected so that they have high enough declinations (table 3.3) to be observed at high elevations from all stations of VLBA. This requirement is essential for successful switching phase-referencing observations at relatively high frequency like 22GHz. Elevation of W3(OH) at each station of VLBA in the first epoch observation is shown in Figure 3.6. It is clear that W3(OH) pair was observed at high elevation except Mauna Kea station.

IRAS21008+4700 is located at $l = 88.8°$ and $b = 0.74°$ and W3(OH) is located at $l = 134.7°$ and $b = 1.07°$ in the Galactic coordinate system (table 3.3). The fact that the both sources are located near the Galactic plane and beyond the Solar Circle is important for the intended further study of the outer rotation curve of the Galaxy.

The peak line-of-sight velocity of IRAS21008+4700 is -50 km/sec and hence the simple flat rotation model of the Galaxy yields a kinematic distance of the source of 7.3 kpc. The widely accepted value of distance to W3(OH) is 2.3 kpc estimated by Georgelin and Georgelin (1976). However, the estimation is based on the old Galactic constraints (R_0 = 10kpc and Θ_0 = 250km s^{-1}), where R_0 is the distance from the Galactic center and Θ_0 is the mean Galactic rotation speed at the Sun. We will discuss the distance of W3(OH) later. These Galacitc water maser sources are likely in Perseus arm (Figure 3.1).

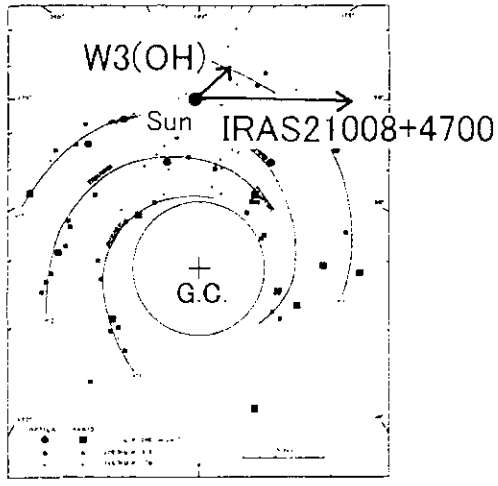

Figure 3.1: Positions of observed Galactic water maser sources in the Galaxy

3.3 Description of Present Observations

IRAS21008+4700 and ICRF2100+468 were observed on July 8 of 1998 for 5 hours and on August 7 of 1998 for 5 hours, while W3(OH) and ICRF0241+622 were observed on November 17 of 1999 for 4 hours and on December 16 of 1999 for 4 hours. The multi-epoch observations are carried out for examination of general repeatability of the results of the observations and for detection of possible displacements of the maser sources within a month. All ten VLBA antennas were successfully operated in the IRAS21008+4700 - ICRF2100+468 pair observations, however, in the W3(OH) - ICRF0241+622 pair observation, St. Croix was not operated due to storm at first epoch and Hancock was not operated due to a azimuth rail trouble at second epoch. System temperature and mean wind speed are shown in Tables 3.4 and 3.5. System temperatures were worse at observation of IRAS2108+4700 and ICRF2100+468 since these observations were made in summer. On the other hand, system temperature of observations of W3(OH) and ICRF0241+622 were better than IRAS pair since these observations were made in winter.

The uv coverages of each observation are shown in Figure 3.2 and 3.3.

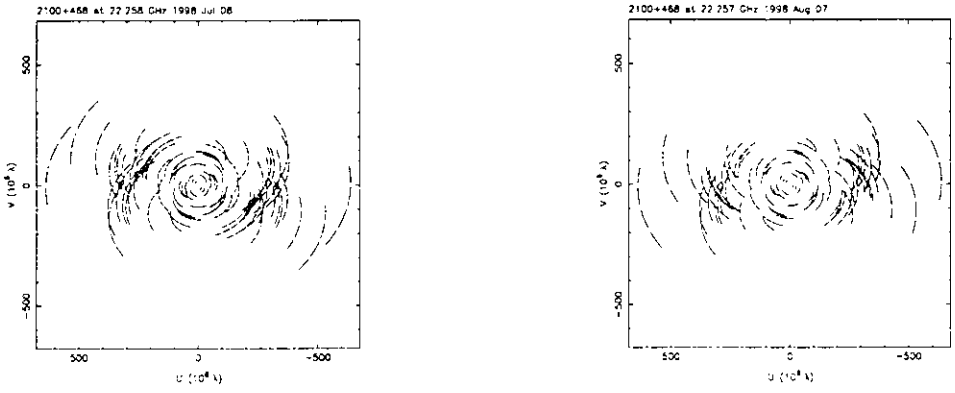

Figure 3.2: UV coverages for IRAS pair

The switching cycle was 40 second in all the observations with typical on-source times shown in table 3.7. The 40 second switching cycle is very

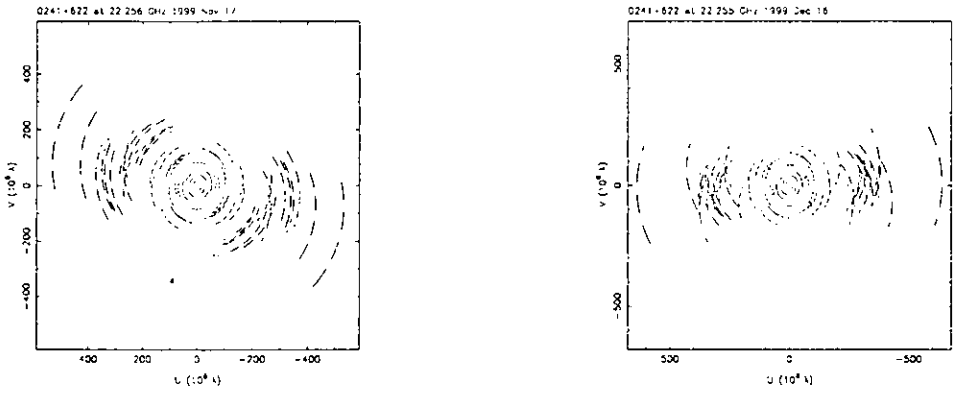

Figure 3.3: UV coverages for W3(OH) pair

Table 3.4: System temp. and Wind speed at IRAS pair observation

Station	System temp.(K)		Mean wind speed (m/h)	
	1st epoch	2nd epoch	1st epoch	2nd epoch
Brewster	150 - 200	130 - 170	0 - 3	0
Fort Davis	120 - 160	90 - 120	0 - 4	0 - 2
Hancock	180 - 220	200 - 250	0 - 2	0 - 1
Kitt Peak	300 - 800	105 - 140	0 - 5	0 - 3
Los Alamos	130 - 170	110 - 150	0 - 3	0 - 2
Mauna Kea	90 - 110	110 - 130	5 - 11	0 - 4
North Liberty	130 - 160	140 - 180	0 - 4	0 - 3
Owens Valley	102 - 120	100 - 140	0 - 3	0 - 3
Pie Town	180 - 440	135 - 170	0 - 3	0 - 3
Sainte Croix 6 130 - 200	120 - 210	1 - 7	0 - 5	

Table 3.5: System temp. and Wind speed at W3(OH) pair observation

Station	System temp.(K)		Mean wind speed (m/s)	
	1st epoch	2nd epoch	1st epoch	2nd epoch
Brewster	150 - 300	134 - 148	0	0
Fort Davis	80 - 90	72 - 78	0 - 1	0 - 3
Hancock	120 - 125	—	0 - 4	—
Kitt Peak	75 - 83	65 - 72	0 - 2	1 - 6
Los Alamos	85 - 95	85 - 95	1 - 3	0 - 3
Mauna Kea	90 - 110	85 - 110	2 - 4	3 - 6
North Liberty	95 - 110	90 - 102	0 - 1	3 - 8
Owens Valley	85 - 95	90 - 110	0 - 7	0 - 4
Pie Town	95 - 110	97 - 105	1 - 3	0 - 3
Sainte Croix	—	90 - 140	—	2 - 8

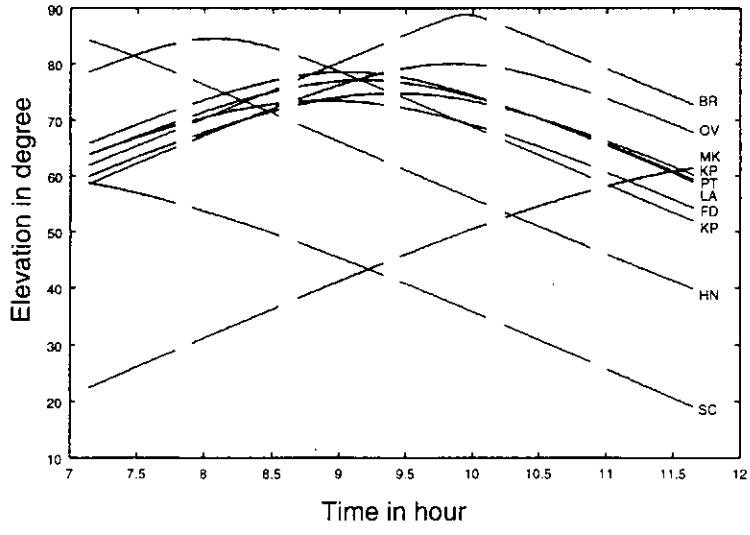

Figure 3.4: Elevation via UT at IRAS21008+4700 pair observation in first epoch

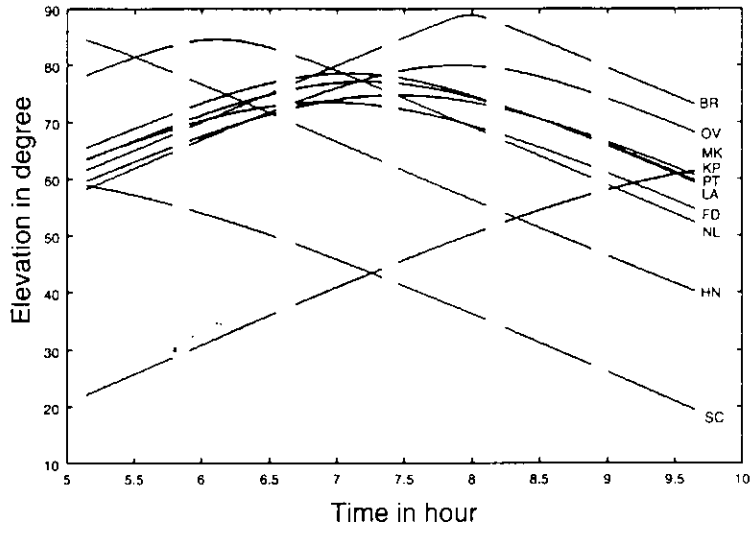

Figure 3.5: Elevation via UT at IRAS21008+4700 pair observation in second epoch

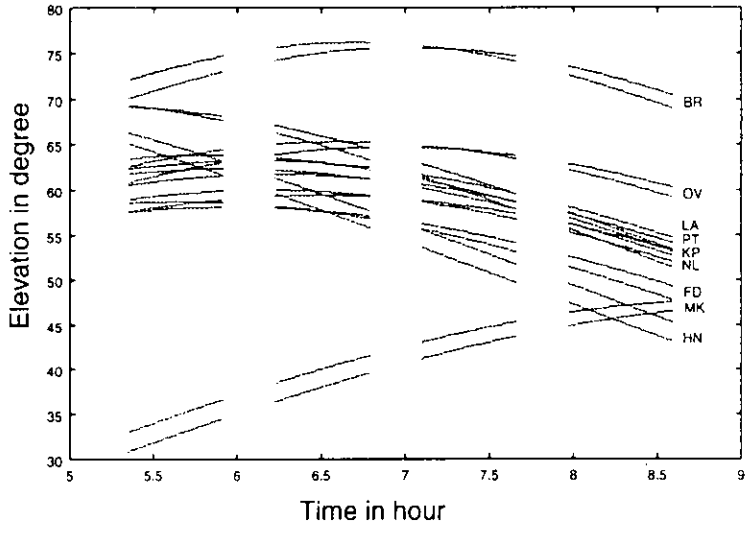

Figure 3.6: Elevation via UT at W3(OH) pair observation in first epoch

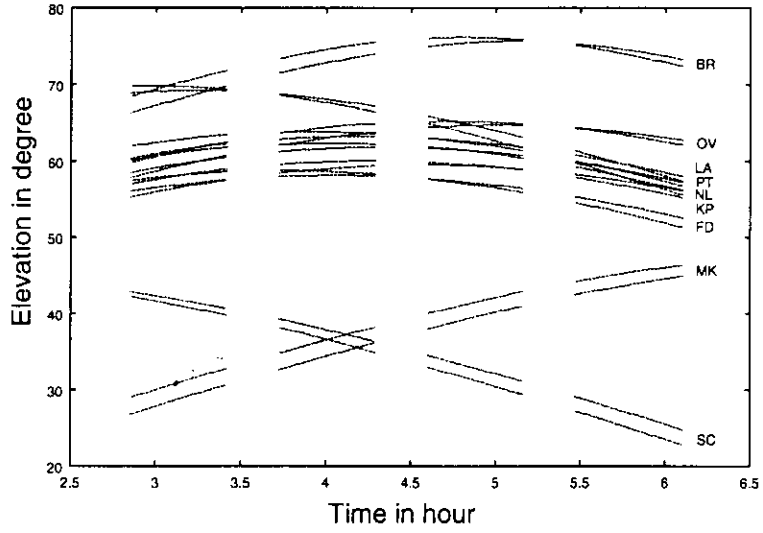

Figure 3.7: Elevation via UT at W3(OH) pair observation in second epoch

short compared with many other phase-referencing VLBI observations performed by VLBA. Also, the value is well shorter than the upper limit of 1.3 minute for successful phase-referencing VLBI observations at 22GHz under normal atmospheric conditions and at 50° elevation, as listed in the VLBA Observer's Guide. However, the short value was chosen on the basis of the simulations of the switching observations made with a statistical model of the excess-path fluctuations in the turbulent troposphere (Sasao 1997). The simulation results showed that the switching cycle should be about 40 second or shorter in order to achieve the highly precise phase difference measurement to be examined in the present study.

The central frequency of the observations was 22.23GHz. The received data of 2 BBC (baseband converter) channels with 16MHz bandwidth each were 2-bit sampled and recorded. The cross-correlation processings were performed in VLBA Correlation Center at Soccoro, NM. The hardware accumulation time was 2 second for all the observations. Number of spectral channels of the correlated data was 1024.

Table 3.6: Separation angle

Target source	Reference source	Separation angle (deg.)
IRAS21008+4700	ICRF2100+468	0.18
W3(OH)	ICRF0241+622	2.17

Table 3.7: Typical on-source time per cycle

Target source	Reference source	on-source time (second)
IRAS21008+4700	ICRF2100+468	15
W3(OH)	ICRF0241+622	8

Chapter 4

Data reduction

The whole process of data reduction was carried out with phase-calibration technique using the NRAO Astronomical Image Processing System (AIPS) package.

4.1 Phase-referencing VLBI data reduction with AIPS

4.1.1 Astronomical Image Processing System (AIPS)

The NRAO Astronomical Image Processing System (AIPS) is a software package for interactive calibration and editing of radio interferometric data and for construction, display and analysis of astronomical images made from those data (Bridle 1994).

In AIPS the visibility (uv) data are kept in multi-source data sets, each of which contains, in time order, visibility data for all sources observed in a session. AIPS follows an incremental calibration process on the multi-source data sets. Gain, fringe-fitting and other calibrations in AIPS create calibration solutions. The calibration solutions are written in SN (Solution) tables, then, calibration (CL) tables are created for improving the visibility data with these calibrations by an AIPS task called CLCAL. Every time when the CLCAL is called a new CL table is created and merged into the

existing CL table created earlier, then forming the cumulative calibration process.

The actual visibilities are not altered until the final calibration which produces single-source data sets that can be imaged.

4.1.2 Phase-referencing VLBI data reduction with AIPS

A flow chart of phase-referencing VLBI data reduction with AIPS is shown in Figure 4.1. The details of reduction steps are as follows.

After loading the VLBI data to the work area of AIPS, amplitude calibration is performed for all observed sources. Next, fringe fitting calibration is made to bright and compact calibrator sources with precisely known celestial positions. Such calibrator sources are specially included in the observing session along with the pair of sources of our interest. The results are used to take out the large delay and fringe rate residuals due to the offsets of clocks and clock rates at antenna sites. Then, fringe fitting is performed again now for one of the sources in the observed pair which is chosen as the reference source (usually an extragalactic source is chosen as the reference) in order to determine the residual delay, fringe rate and fringe phase of the reference source and store them in the calibration table. Now the phase-referencing with AIPS is realized by applying the calibration table obtained for the reference source in the second fringe fitting to the target source (usually a Galactic maser source). The residual fringe phase determined for the reference source in the second fringe fitting contains the phase fluctuations due to the irregular atmospheric refraction and instability of the observing system. But these effects should be almost equally included in the fringe phase of the adjacent target source as well. Therefore, by applying the calibration table determined for the reference source to the target, we can largely eliminate the degrading effects of the atmospheric and instrumental phase fluctuations. Moreover, since the residual fringe phase determined in the second fringe fitting also contains the component due to the error in the adopted celestial position of the reference source, this procedure effectively defines the true position of the reference source as a reference point for the

position determination of the target source. Thus, after the calibration, the fringe phase of the target source must mostly include only the information of its relative position with respect to the reference position. Therefore, by drawing the image of the target source with AIPS and determining positions of the maser spots on the image map by one Gaussian component fit, we obtain highly precise positions of the maser spots with respect to the reference source position. In the present analysis the images of the maser spots were fairly simple and consistent with the synthesized beam pattern. Therefore, we applied the simple one Gaussian component fit for the position determination. In the course of the Gaussian fitting, the peak intensity, the position of the intensity peak, the major axis, the minor axis and the position angle of the Gaussian components are estimated with their statistical fitting errors.

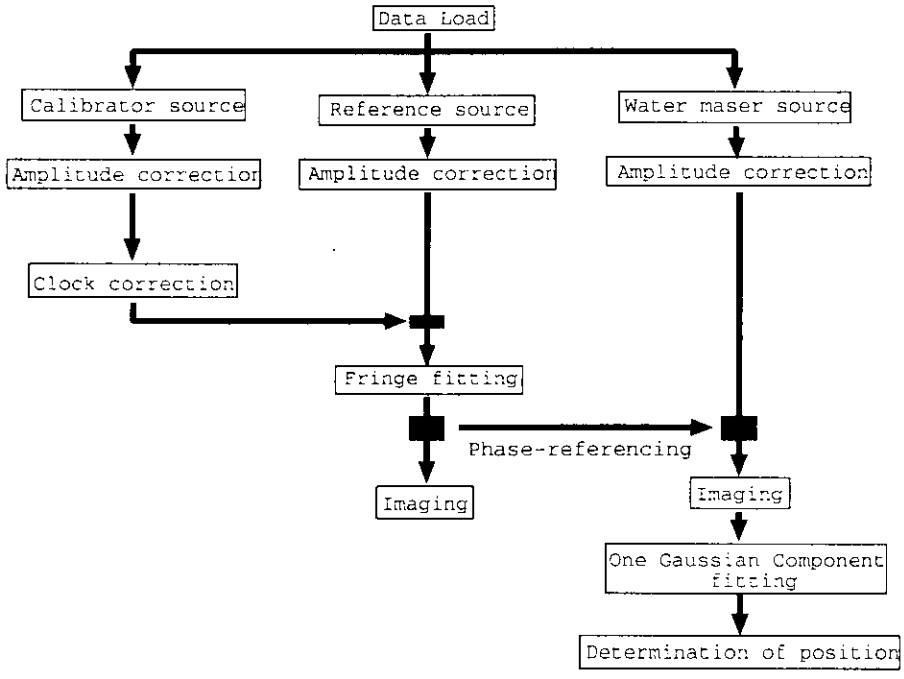

Figure 4.1: The flow chart of the present data reduction using phase-referencing technique with AIPS

Chapter 5

Results

5.1 Removal of atmospheric phase fluctuation

We now examine how well the compensation of atmospheric and instrumental fluctuations of fringe phase was performed in the present phase-referencing VLBI observation. For that purpose, we take pair of W3(OH) and ICRF0241+622 which are both strong.

Figure 5.1 shows time behaviour of 2-second(hardware accumulation time) values of fringe phases for a maser feature with V_{LSR} = -46.48 km s^{-1} and ICRF0241+622 obtained at North Liberty - Pie Town baseline (1663km) in the first epoch observation. Since both sources are bright enough and baseline sensibility is high, thermal noise fluctuation is fairly small . In fact, the thermal noise phase fluctuation of the weaker source ICRF0241+622 was only 9 degrees. Therefore, we can well trace the time behaviour of the fringe phase.

In order to show the time behaviour more clearly, we connected in Figure 5.2 360° jumps in the phase time series. The three wide gaps in the time series of fringe phase came from observing calibrator source.

The systematic decrease of the fringe phase of the maser feature is due to offset in its position from the tracking center. In Figure 5.3 a linear trend is subtracted from W3(OH) phase for roughly removing the systematic

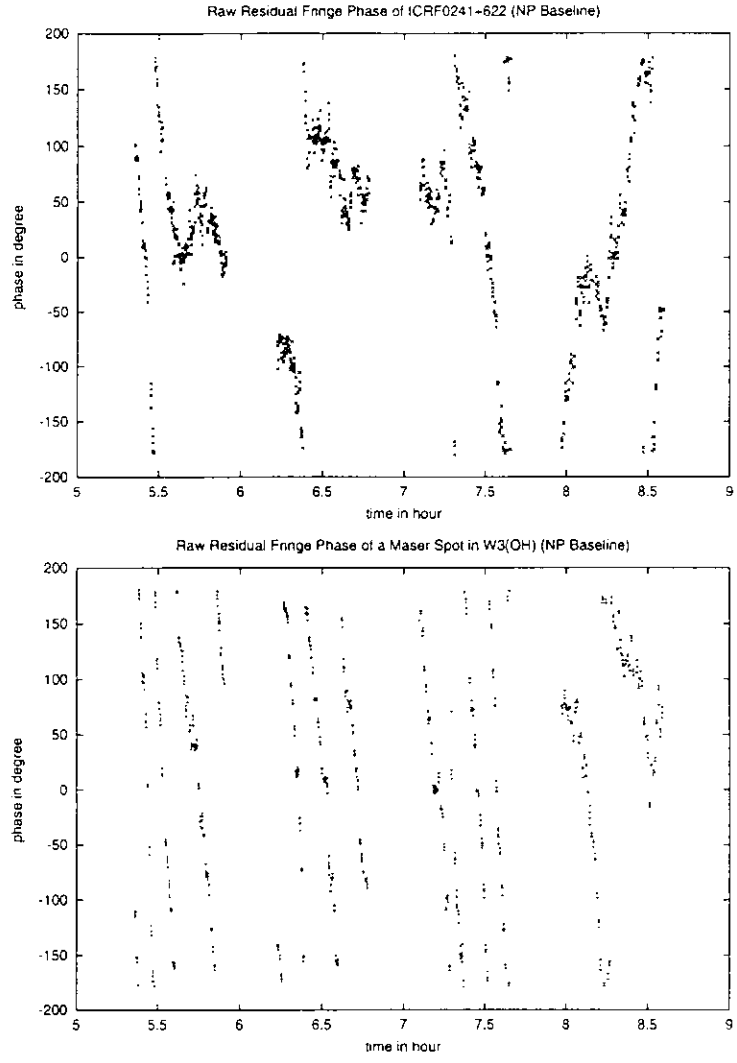

Figure 5.1: Raw Residual Fringe Phase of maser spot in W3(OH) and ICRF0241+622 (North Liberty - Pie Town Baseline).

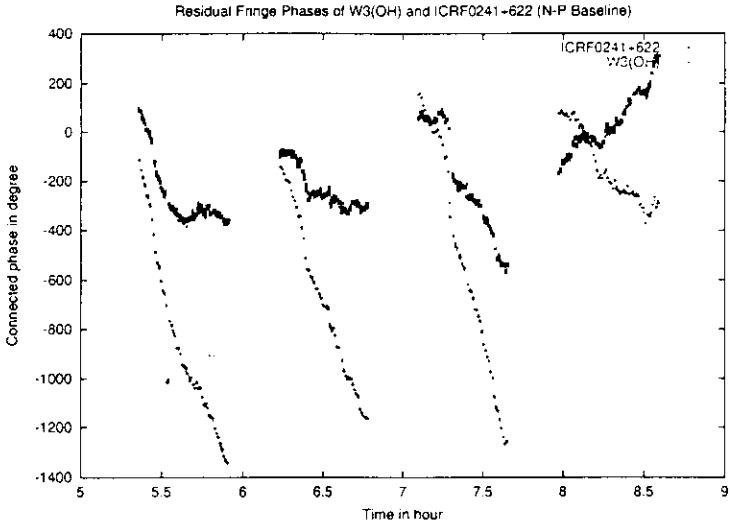

Figure 5.2: Raw Residual Fringe Phase of maser spot in W3(OH) and ICRF0241+622 (North Liberty - Pie Town Baseline) after connection 360° jumps in the phase time series.

decrease. Now it is evident from the figure that time behaviour of the maser and reference sources are quite similar.

Figure 5.4 shows difference of the fringe phases of the maser and reference sources presented in Figure 5.2. The phase difference exhibits very smooths time variation. It is thus clear that the common large time variations due to the atmosphere and instrument instability are mostly removed in the phase-referencing as discussed in Chapter 2. The amount of residual phase fluctuations will be discussed later in Chapter 6.

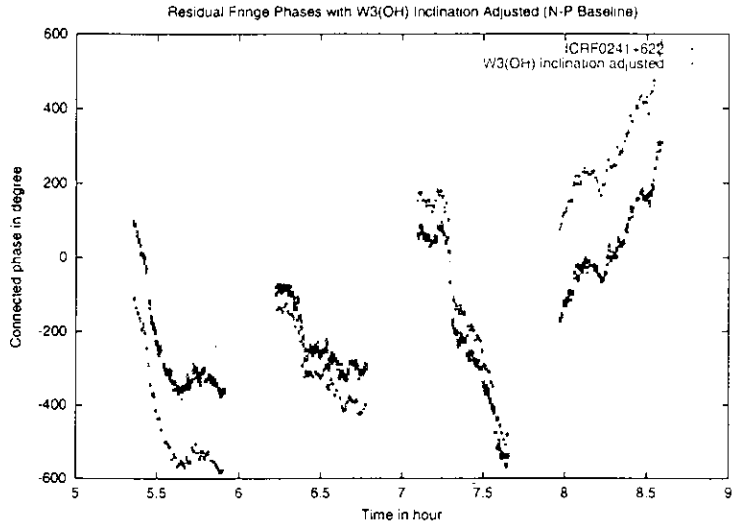

Figure 5.3: Raw Residual Fringe Phase of maser spot in W3(OH) and ICRF0241+622 (North Liberty - Pie Town Baseline) after subtraction of linear trend of W3(OH) phase.

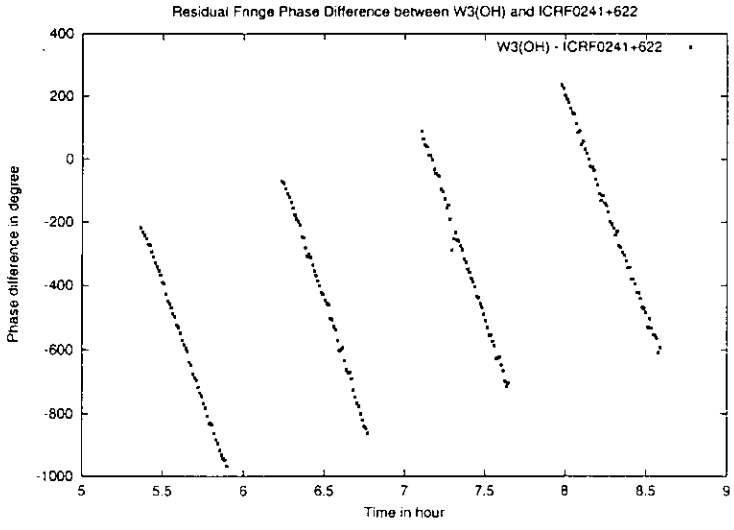

Figure 5.4: Difference of Fringe Phase of maser spot in W3(OH) and ICRF0241+622 (North Liberty - Pie Town Baseline).

5.2 Results for IRAS21008+4700 and ICRF2100+468 pair

5.2.1 ICRF2100+468

Reference source, ICRF2100+468 was detected in both epochs. Figure 5.2.1 shows the image maps of the source at two epochs of the observation. The source images are fairly consistent with the synthesized beam pattern. We will discuss the effect of the source structure to the position determination in Chapter 6.

Derived correlated peak intensity of the source at 22GHz was 0.128 Jy/beam at first epoch and 0.122 Jy/beam at second epoch.

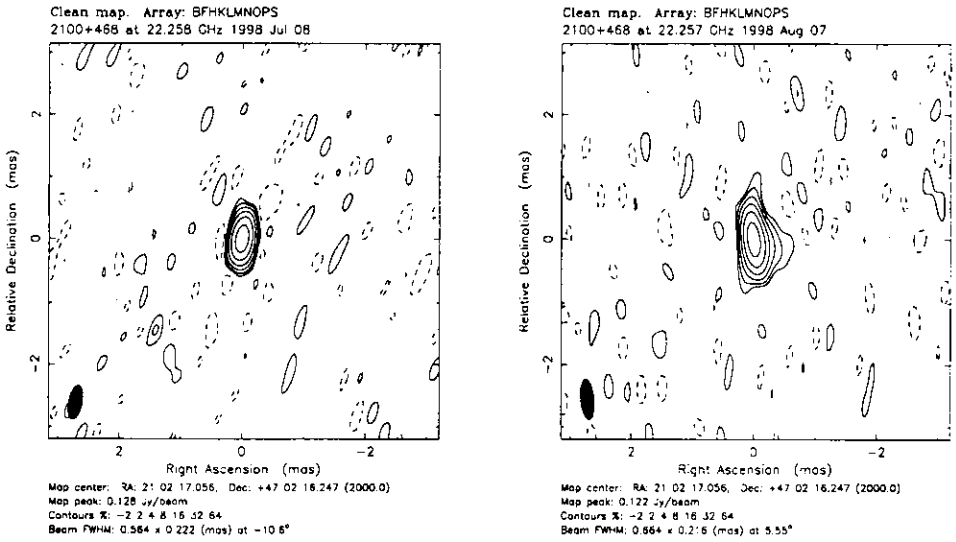

Figure 5.5: The images of ICRF2100+468 in two epochs of observations.

5.2.2 Detection of proper motions of IRAS21008+4700

We detected two maser features in both epochs. They are separated by about 150 mas in east-west direction. The LSR velocities of these maser features are around -36km s^{-1} and -71km s^{-1}, respectively. The maser features usually consist of several spots, or velocity components(Gwinn, 1994).

Table 5.1: Proper motions of IRAS21008+4700 relative to ICRF2100+468.

Velocity(LSR) (LSR) ($km\ s^{-1}$)	RA offset (mas)	Dec offset (mas)	Displacement (mas)	Error (mas)	Position angle (deg)	Error (deg)	Peak Intensity 1st epoch (Jy/beam)	second epoch (Jy/beam)
-36.98	-55.475	78.09	0.500	0.063	138.7	0.1	0.35	0.68
-36.77	-55.394	78.09	0.516	0.033	132.7	0.1	0.45	1.1
-36.56	-55.397	78.01	0.443	0.024	125.8	0.1	0.56	1.1
-36.35	-55.449	78.09	0.493	0.041	135.2	0.1	0.37	0.93
-36.14	-55.406	78.03	0.318	0.062	125.0	0.2	0.26	0.56
-35.95	-55.377	78.17	0.423	0.084	101.3	0.4	0.17	0.30
-71.63	88.557	39.54	0.350	0.049	125.0	0.2	0.33	0.59
-71.42	88.514	39.61	0.422	0.056	141.8	0.1	0.49	0.60
-71.21	88.534	39.62	0.347	0.066	135.9	0.2	0.67	0.57
-71.00	88.526	39.60	0.318	0.118	132.7	0.4	0.48	0.43

The LSR velocities of the maser spots in both of the features and their correlated peak intensities are listed in Table 5.1.

Maser spots showing the same LSR velocities at both epochs are identified as the same spots. Their displacements in the sky with respect to ICRF2100+468 during a month are shown in Table 5.1 and Figure 5.6. Uncertainty (statistical error) in the measured displacement of a maser spot was estimated in AIPS by the one Gaussian component fit in the image map and is typically several tens μas. The detected proper motions of spots with peak intensity within each maser feature is $\mu v_{LSR=-36.56 kms^{-1}} = 443 \pm 24 \mu$as with position angle of 125.8 ± 0.1 degree and $\mu v_{LSR=-71.21 kms^{-1}} = 347 \pm 66 \mu$as with position angle of 135.9 ± 0.2 degree, respectively (Table 5.1).

These maser features were separated by about 150 mas at both epochs. Moreover, this separation was increased during a month with approximately keeping their position angle (Table 5.2). This extension suggests that these maser spots were associated with jet or bipolar outflow of 1000 AU scale with velocity of 54.1 ± 21.4 km/s at assumed distance of 7.3 kpc. (Figure 5.7).

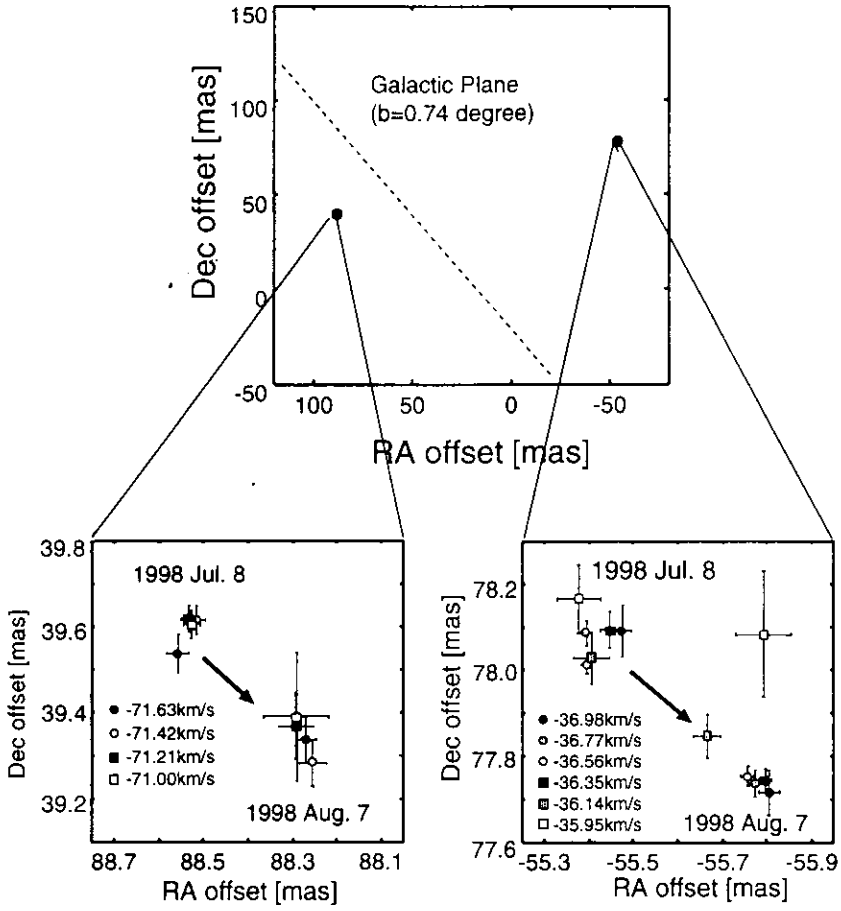

Figure 5.6: Displacements of maser features in IRAS21008+4700 relative to adjacent extragalactic source ICRF2100+468. Top panel shows the wide view of the location of two spots in IRAS21008+4700. Dashed line is parallel to the Galactic plane (b=+0.41°). Lower two panels show the proper motions of the features. Arrows show directions of the movements. Note that both of them are almost parallel to the Galactic plane.

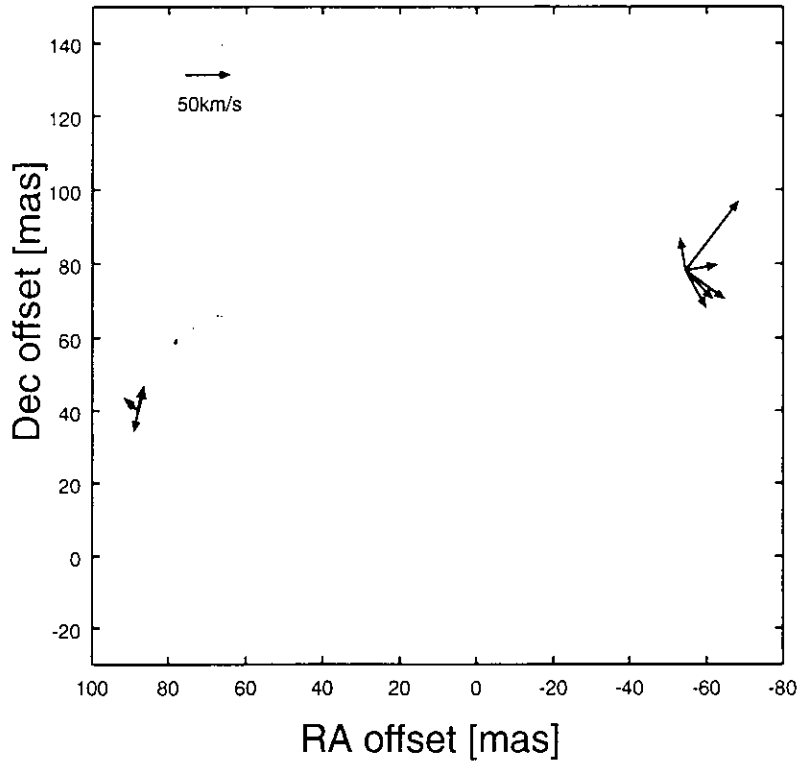

Figure 5.7: The internal motion of maser spots in IRAS21008+4700. Systematic motion due to the Galacitc rotation, annual parallax and Solar motion was subtracted beforehand according to the model to be described in Chapter 7.

Table 5.2: Intrinsic motions of IRAS21008+4700

Epoch	Separation angle (mas)	Position angle (deg)
hline July 8 1998	148.964±0.022	75.0560±0.0002
August 7 1998	149.075±0.046	75.0715±0.0005

5.3 Results for W3(OH) and ICRF0241+622 pair

5.3.1 ICRF0241+622

Reference source, ICRF2041+622 was detected in both epochs. The peak intensity of ICRF0241+622 was 0.589 Jy/beam at first epoch and 0.482 Jy/beam at second epoch. The image maps at two epochs are shown in Figure 5.3.1.

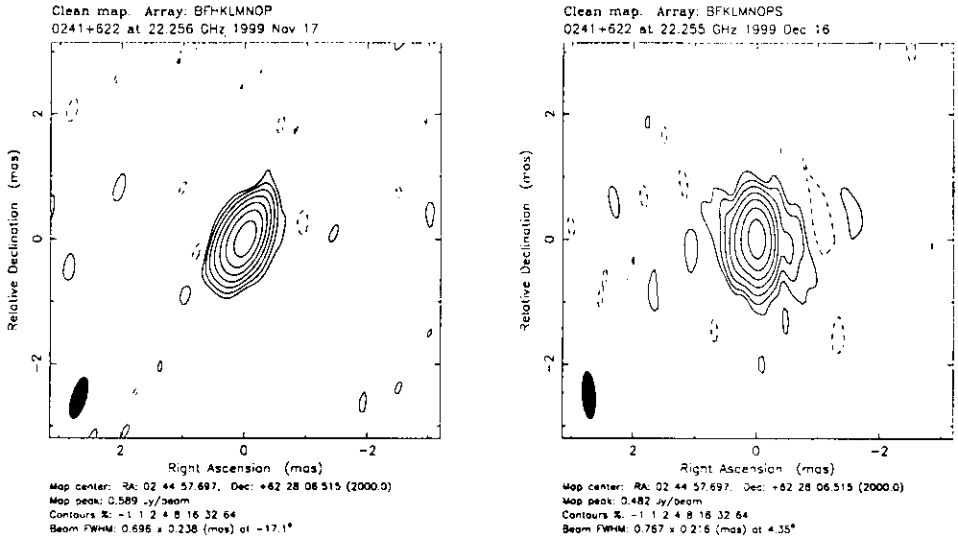

Figure 5.8: The image of ICRF0241+622

5.3.2 Detection of proper motions of W3(OH)

We detected about 40 maser features in both epochs (Table 5.3 and Figure 5.9).

The features are spread over a region of about 2300 mas × 400 mas. Their distribution was generally similar to those reported in earlier VLBI observations (ex. Alcolea et al, 1992).

The proper motions of the features relative to ICRF0241+622 during a month are detected for the maser features showing the same LSR velocities in both epochs and are listed in Table 5.3. The cross-correlation spectra of

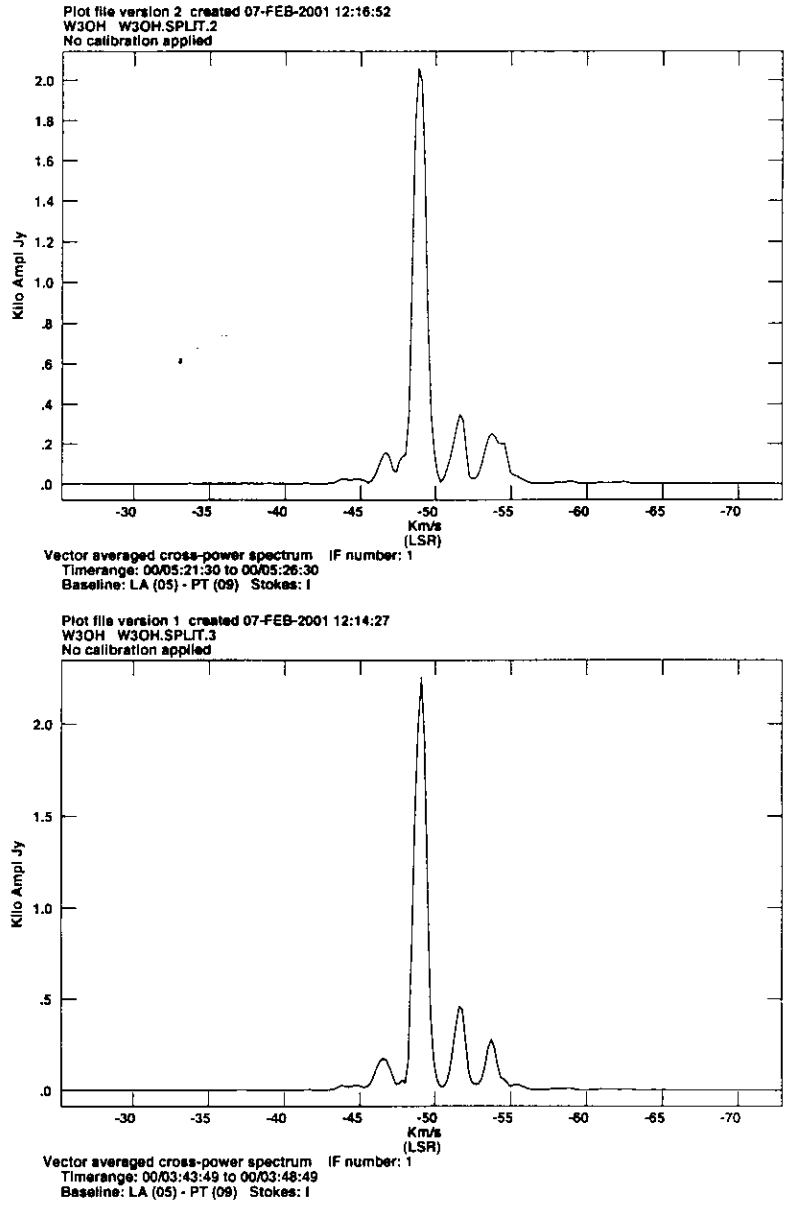

Figure 5.9: Cross correlated power spectrum of the 22 GHz H_2O maser emission in W3(OH). Upper panel shows the spectrum at first epoch (Nov. 1999). Lower panel shows the spectrum at second epoch (Dec. 1999).

W3(OH) features at two epochs are shown in Figure ??. The uncertainty (statistical error) of the derived displacement of each feature was estimated by the one Gaussian component fitting. They range from 7 μas to 232 μas. Median of the displacements of maser spots in W3(OH) is $\mu = 338 \pm 22\mu$as with position angle of 121.4 $\pm$ 0.1 degree.

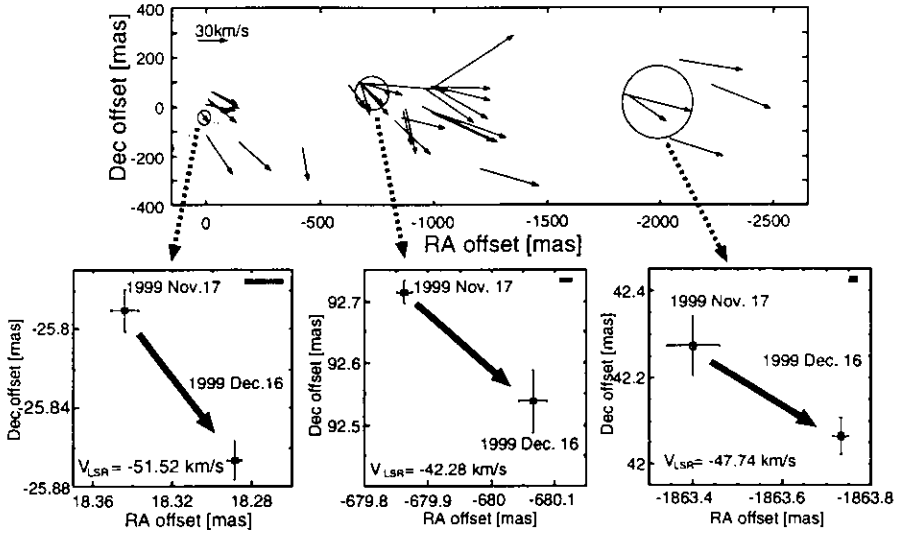

Figure 5.10: The transversal velocities of water maser features in W3(OH) relative to adjacent extragalactic source ICRF0241+622. A distance of 2.3kpc (Georglin and Georglin, 1976) has been assumed. Lower panels show displacements of three maser features.

5.3.3 Statistical parallax of W3(OH) using water maser spots

It is possible to determine distance of a maser source with VLBI by comparing detected proper motions and radial velocities within a group of maser features (Genzel et al, 1981a) . This method requires that both radial and proper motions are kinematic, and that the number of features with measured motions is large (typically N $\geq$ 20).

If the motions are predominantly random, as in a turbulent velocity field, one can compare the velocity dispersion in the radial direction (σ_{v_z} [km s^{-1}])

Table 5.3: Proper motions of W3(OH) relative to ICRF0241+622

Velocity(LSR) (km s^{-1})	Displacement (mas)	Error (mas)	Position angle (deg.)	Error (deg.)
-42.29	0.297	0.043	120.3	0.2
-46.48	0.094	0.013	143.9	0.1
-47.74	0.270	0.029	100.2	0.2
-47.53	0.307	0.051	126.2	0.2
-48.79	0.260	0.012	115.8	0.1
-49.42	0.216	0.027	127.1	0.1
-50.89	0.409	0.029	144.2	0.1
-51.52	0.375	0.010	129.7	0.0
-60.76	0.184	0.017	115.3	0.1
-43.75	0.235	0.013	141.6	0.1
-49.84	0.410	0.094	104.9	0.4
-50.26	0.390	0.092	136.0	0.2
-52.15	0.254	0.104	161.2	0.5
-52.15	0.283	0.035	171.0	0.1
-54.46	0.277	0.019	164.4	0.0
-55.30	0.769	0.232	94.6	0.2
-55.72	0.269	0.041	131.1	0.2
-50.89	0.557	0.093	105.0	0.3
-51.94	0.491	0.038	123.3	0.1
-53.41	0.554	0.010	102.9	0.0
-55.93	0.594	0.079	113.4	0.2
-56.77	0.584	0.110	118.4	0.3
-56.77	0.677	0.027	107.5	0.1
-58.87	0.516	0.007	91.5	0.0
-57.19	0.419	0.043	103.2	0.1
-57.61	0.065	0.029	114.1	0.7
-57.82	0.430	0.020	130.9	0.0
-59.92	0.291	0.023	164.4	0.0
-60.97	0.391	0.078	166.3	0.2
-62.02	0.803	0.080	59.4	0.1
-66.17	0.739	0.041	113.4	0.1
-43.12	0.580	0.013	98.1	0.0
-45.22	0.500	0.008	106.8	0.0
-50.26	0.609	0.064	102.8	0.1
-56.98	0.393	0.010	122.1	0.0
-62.23	0.568	0.007	110.2	0.0

with that in the proper motion coordinates (σ_μ [rad s^{-1}]). If all velocity components are normally distributed with the same velocity dispersion, the distance D can be estimated from

$$D = \frac{\sigma_{v_z}}{\sigma_\mu}. \tag{5.1}$$

This is the method of Statistical Parallax, well known in stellar statistics. In order to find the true proper motion dispersion σ_μ from the observed value $\sigma_\mu^{\rm obs}$, one has to correct for the broadening of the observed dispersion by the finite measurement accuracy e_μ of the proper motions with the formula

$$\sigma_\mu^2 = \left(\sigma_\mu^{\rm obs}\right)^2 - e_\mu^2. \tag{5.2}$$

On the other hand, the accuracy to which distance can be estimated by this method is

$$\sigma_{\rm D} \approx \left[\frac{1}{4N}\left[\frac{2N}{M} + \left[1 - \left(\frac{e_\mu}{\sigma_\mu^{\rm obs}}\right)^{-1}\right]\right]\right]^{\frac{1}{2}} \tag{5.3}$$

where N is the number of maser features with measured transverse motions, and M is the number of features with measured radial velocities. In the present case, N = M = 36, since proper motions were detected for all maser features.

In the present observation, the statistical parallax distance to W3(OH) was estimated as 3.33 $\pm$ 0.49 kpc using equation (5.2). We will discuss the distance to W3(OH) later in Chapter 7.

The mean displacements were $\mu_{\Delta\alpha} = -0.338$ mas/month and $\mu_{\Delta\delta} = -0.162$ mas/month, respectively. If we assume the residual displacements of the maser features from the mean displacements as Gaussian random variables, we can estimate the uncertainties of the maser displacements as $\sigma_{\mu_{\Delta\alpha}} = 0.069$ mas/month and $\sigma_{\mu_{\Delta\delta}} = 0.036$ mas/month, respectively. Therefore, the mean proper motion of maser features in W3(OH) region derived from observation is likely to have the uncertainty of this level (Figure 5.11).

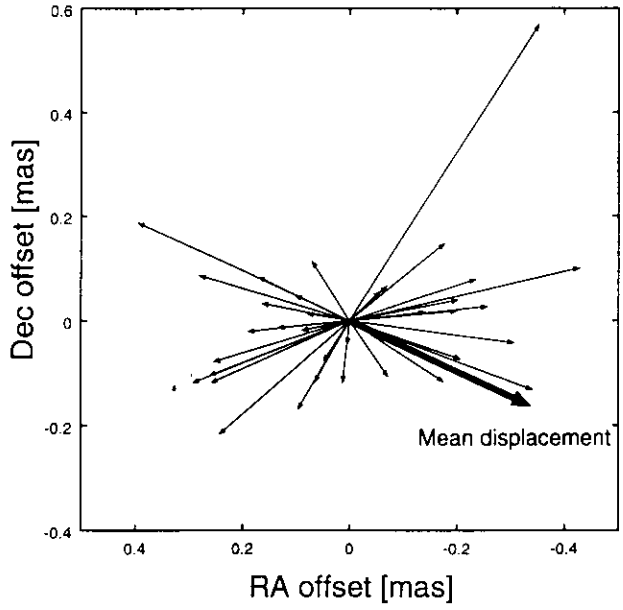

Figure 5.11: The residual displacement

The internal motions of maser features after the subtraction of the mean motion in W3(OH) are shown in Figure 5.12. They are consistent with the East–West bipolar outflow reported in previous observations (Alcolea et al., 1992).

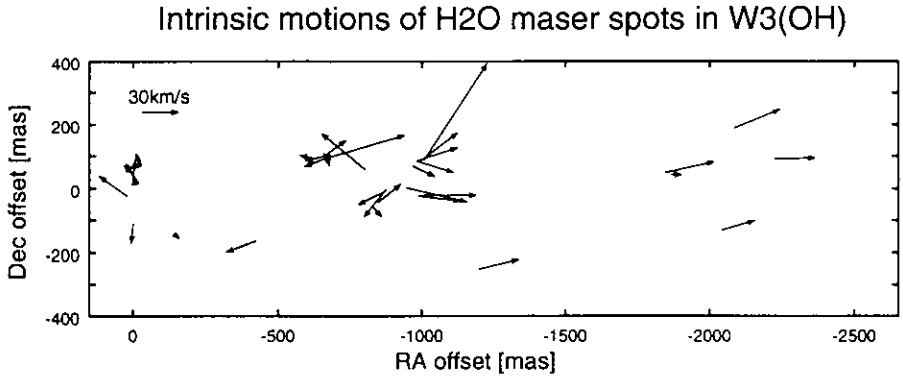

Figure 5.12: The internal motion of W3(OH). A distance of 2.3kpc (Georglin and Georglin, 1976) has been assumed.

Chapter 6

Error estimation

6.1 Statistical errors and systematic errors

Now we estimate errors contained in the present results. We will consider the problem on the basis of equations (2.11) shown in Chapter 2. Equation (2.11) can be expressed as

$$\begin{aligned}\phi^{targ} - \phi^{ref} &= 2\pi\nu\frac{\mathbf{D}_0 \cdot \left(\Delta\mathbf{s}^{\mathrm{targ}} - \Delta\mathbf{s}^{\mathrm{ref}}\right)}{c} + 2\pi\nu\frac{\Delta\mathbf{D} \cdot \left(\mathbf{s}_0^{\mathrm{targ}} - \mathbf{s}_0^{\mathrm{ref}}\right)}{c} \\ &+ \left(\phi_{\mathrm{stru}}^{\mathrm{targ}} - \phi_{\mathrm{stru}}^{\mathrm{ref}}\right) \\ &+ \left(\phi_{\mathrm{atmo}}^{\mathrm{targ}} - \phi_{\mathrm{atmo}}^{\mathrm{ref}}\right) + \left(\phi_{\mathrm{inst}}^{\mathrm{targ}} - \phi_{\mathrm{inst}}^{\mathrm{ref}}\right) \\ &+ (\text{thermal noise})^{\mathrm{targ}} + (\text{thermal noise})^{\mathrm{ref}} \end{aligned} \tag{6.1}$$

The left hand side of this equation stands for the fringe phase difference observable. The first term in the right hand side contains the relative position between the target and reference sources which is the parameter to be estimated. Other terms in the right hand side include baseline errors, source structure effect, atmospheric and instrumental phase fluctuations and thermal noise. All of them could be sources of errors for the relative position measurement.

The error sources can be divided into two categories. One category includes error sources which cause irregular variations of the phase difference

with time scales shorter than the time scale of the observation. In the Gaussian fitting of the radio source image performed in AIPS, the short-time-scale phase variations act as noise and contribute to the statistical fitting error estimated by AIPS. In equation (6.1), most of the atmospheric and instrumental phase fluctuations and thermal noise in 4-th, 5-th and 6-th terms in the right hand side are the sources of the statistical error.

Error sources of the another category have time scales longer than the time scale of the observation. They are not treated as noise in the Gaussian fitting and instead included in the estimated values of the searched parameters thus deviating the estimation. We call such errors as systematic errors. In the right hand side of equation (6.1), the baseline errors in the second term and most of the radio source structure effect in the third term belong to this category.

Here we will examine 1) whether the estimation of the statistical error given by AIPS is appropriate and 2) how the systematic error affects the astrometric results obtained in the present study.

6.2 Reliability of estimated statistical error

6.2.1 Thermal noise error

If we denote the signal-to-noise ratio of an observation as SNR, the thermal noise error in the fringe phase measurement can be estimated by a simple formula

$$\sigma_{thermal} = \frac{1}{SNR} \qquad (radian), \tag{6.2}$$

when $SNR \gg 1$, while the SNR itself is estimated by

$$SNR = \frac{\pi}{8\kappa}\eta\frac{S_\nu\sqrt{\eta_{A_i}\eta_{A_j}}L_iL_j\sqrt{2B\tau_a}}{\sqrt{T_{s_i}T_{s_j}}} \tag{6.3}$$

(Thompson et al., 1986), where κ is Boltzmann constant, η is coherence factor, S_ν is flux density of source, η_{A_i} is aperture efficiency for i th antenna, L_i is a diameter of i th antenna, B is total band width, τ_a is integration time and T_{s_i} is system noise temperature for i th antenna.

	first epoch	second epoch
IRAS21008+4700	0.56	1.1
ICRF2100+468	0.128	0.122
W3(OH)	2000	2000
ICRF0241+622	0.589	0.482

Table 6.1: Peak intensity (Jy/beam)

We adopt following representative values in the present observations to estimate the thermal noise error.

$T_s = 100K$ for W3(OH)-ICRF0241+622 pair (winter)
$T_s = 150K$ for IRAS21008+4700-ICRF2100+468 pair (summer)
$\eta = 0.8$
$\eta_A = 0.66$
$L = 25$ m
$B = 32$ MHz for continuum sources
$B = 16$ kHz for maser sources
$\tau_a = 24$ sec for W3(OH)-ICRF0241+622 pair
$\tau_a = 45$ sec for IRAS21008+4700-ICRF2100+468 pair

The integration times correspond to the three times of the on-source times (8 seconds for W3(OH)-ICRF0241+622 pair and 15 seconds for IRAS21008+4700-ICRF2100+468 pair, respectively) within a switching cycle (40 seconds). Three times of the switching cycle, 120 seconds, corresponds to the typical VLBI coherence time at 22 GHz.

The peak intensity in Jy/beam at the two epochs of observations are listed in Table 6.1.

Estimated SNR values and thermal noise phase errors per beam for a baseline are listed in Tables 6.2 and 6.3.

The thermal noise errors in the phase difference of W3(OH)-ICRF0241+622 pair which is the root square sum of the values listed in Table 6.3 are 2.6 and

	first epoch	second epoch
IRAS21008+4700	0.42	0.83
ICRF2100+468	4.3	4.1
W3(OH)	1600	1600
ICRF0241+622	22	18

Table 6.2: Signal to noise ratio per beam

	first epoch	second epoch
IRAS21008+4700	136	69
ICRF2100+468	13	14
W3(OH)	0.036	0.036
ICRF0241+622	2.6	3.2

Table 6.3: Thermal noise phase error per beam (degree)

3.2 degrees for the first and second epochs, respectively. If we adopt as a typical projected baseline length 4000 km, the errors in the phase difference values integrated for the time interval as short as 120 second correspond to about 5 μas error only in the relative position measurement in the sky. Since the thermal error decreases as inverse square root of time in the coherent phase-referenced integration, the thermal noise contribution to the final relative position estimation must be negligibly small compared with the statistical fitting errors given by AIPS.

Although the thermal noise phase error in IRAS21008+4700–ICRF2100+468 pair is much larger (136 degrees in 120 second integrated value), the error must be suppressed down to 14 degrees after the phase-referenced integration for three hours of the observation. The 14-degree phase error corresponds to about 26 μas position error for 4000 km projected baseline.

Therefore, the thermal noise phase error is not a dominating factor in the statistical fitting error for W3(OH)–ICRF0241+622 pair and is in the same level as the fitting error for IRAS21008+4700–ICRF2100+468 pair.

6.2.2 Atmospheric and instrumental errors

The successful removal of the atmospheric and possible instrumental phase fluctuations was demonstrated in the previous chapter. The results were obtained in the bright pair of W3(OH) and ICRF0241+622 for which the time behaviors of the fringe phases were clearly traced. The similar compensation of the phase fluctuations is expected for IRAS21008+4700–ICRF2100+468 pair as well, though the sources are too weak to explicitly get the phase time series.

Figure 6.1 shows 40 second running mean phase difference time series for North Liberty–Pie Town baseline (1663 km) at the first epoch observation of W3(OH)–ICRF0241+622 pair after the phase-referencing calibration performed in AIPS. The rms residual phase difference of the 40 second averaged values is about 9.7 degrees. Since the residual phase contains the thermal noise contribution discussed above, this value gives a crude upper limit for atmospheric and instrumental phase fluctuations after successful

phase-referencing. The 9.7-degree error corresponds to 18 μas error in the sky.

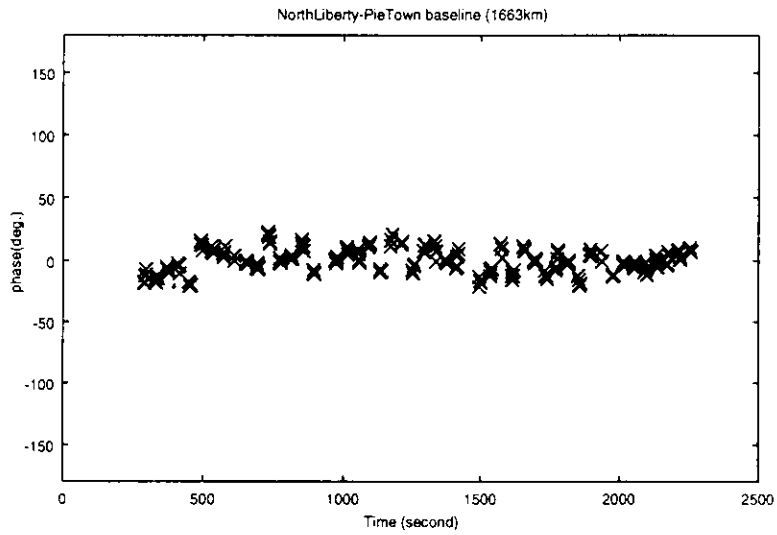

Figure 6.1: The residual phase of a maser feature in W3(OH) after phase-referencing

In the light of the above examination of the residual phase fluctuations and the estimation of the thermal noise error, it is concluded that the quoted statistical fitting errors of several tens micro arcseconds are reasonable.

6.3 Systematic errors

6.3.1 Baseline error

The phase errors induced by the baseline errors (i.e. errors in the positions of antennas on the surface of the Earth and their unpredictable displacements due to the irregular rotation of the Earth) cause errors in the measurements of the source position. It is evident from equation (2.4) and (2.5) , that the source position error $\Delta\phi_{\text{baseline error}}$ can be roughly estimated in terms of the baseline error ΔD and angular separation of the sources θ as

Site Name	X (m)	Y (m)	Z(m)	σ_X (m)	σ_Y (m)	σ_Z (m)
	V_X (m/s)	V_Y (m/s)	V_Z (m/s)	σ_{V_X} (m/s)	σ_{V_Y} (m/s)	σ_{V_Z} (m/s)
Owens Valley	-2410421.308	-4477800.374	3838690.277	.004	.007	.006
	-.0166	.0071	-.0086	.0004	.0005	.0005
Fort Davis	-1330008.188	-5328391.585	3236502.700	.002	.003	.003
	-.0127	-.0025	-.0070	.0003	.0004	.0003
Pietown	-1640953.707	-5014816.028	3575411.870	.001	.002	.002
	-.0144	-.0024	-.0086	.0003	.0003	.0004
Los Alamos	-1449752.356	-4975298.593	3709123.916	.001	.002	.002
	-.0136	.0000	-.0082	.0003	.0004	.0004
North Liberty	-130872.249	-4762317.122	4226851.030	.001	.002	.002
	-.0149	.0006	-.0054	.0003	.0004	.0004
Kitt Peak	-1995678.625	-5037317.718	3357328.118	.001	.002	.002
	-.0131	.0000	-.0096	.0004	.0006	.0005
Hancock	1446375.124	-4447939.660	4322306.112	.001	.002	.002
	-.0150	-.0010	.0000	.0004	.0007	.0007
Brewster	-2112064.973	-3705356.517	4726813.788	.001	.002	.002
	-.0135	.0010	-.0119	.0004	.0005	.0005
Mauna Kea	-5464074.965	-2495249.115	2148296.831	.002	.002	.002
	-.0143	.0612	.0288	.0007	.0006	.0006
Sainte Croix	2607848.532	-5488069.699	1932739.525	.002	.003	.002
	.0093	.0045	.0106	.0005	.0010	.0006

Table 6.4: Positions and velocities of VLBA stations at epoch 1997.0 given in ITRF97

$$\Delta\phi_{\text{baseline error}} = \frac{2\pi\nu}{c}(\Delta \mathbf{D}\theta)\,. \tag{6.4}$$

Table 6.4 lists positions and velocities of VLBA stations at epoch 1997.0 determined in the International Terrestrial Reference System called ITRF97. From this table, we take 7 mm as the worst case of the baseline error. Then equation (6.4) yields phase errors as listed in Table 6.5.

Therefore, the baseline errors of VLBA stations are likely to cause the astrometric errors of about 13 μas for 4000 km projected baseline.

Table 6.5: Phase error due to baseline error

Target source	Reference source	Separation angle (deg.)	phase error (deg.)
IRAS21008+4700	ICRF2100+468	0.18	0.59
W3(OH)	ICRF0241+622	2.17	7.1

Table 6.6: RMS phase delay due to the source structure

Reference source (epoch)	residual delay (ps)	phase error (degree)
ICRF2100+468 (Jul. 1988)	6.51	52.0
ICRF2100+468 (Aug. 1998)	5.74	45.9
ICRF0241+622 (Nov. 1998)	6.26	50.1
ICRF0241+622 (Dec. 1998)	6.18	49.3

6.3.2 Reference source structure effect

Now we examine the source structure effect in the second term of the right hand side of equation (6.1. The phase error due to the source structure is expressed by equation (2.6). Therefore, the source structure effect on the phase delay is

$$\tau_{\rm stru} = \frac{1}{2\pi\nu} \arg\left(\int\int I(x,y) e^{-i2\pi(ux+vy)}\, dx\, dy \right). \qquad (6.5)$$

Using a computer code developed by Dr. Satoko Sawada-Satoh (private communication), we calculated the phase delay for each u, v point for the brightness distributions of the reference sources obtained in the present observations. Then we took the root mean square of the phase delay values over the uv area of $(6 \times 10^8\lambda) \times (6 \times 10^8\lambda)$, where λ is the wave length, to see the extent of the structure effect in the real VLBA observations. The RMS value gives a measure of the phase delay error to be encountered at an arbitrary uv point. The results are shown in Table 6.6.

It is evident from the table that the source with apparently simple structure may cause the phase error as large as 50 degrees corresponding to the celestial position error exceeding 100 μas.

The closure phases of the bright reference source ICRF0241+622 in the two epochs are shown in Figures 6.2. It is evident that the standard deviation of the closure phase of ICRF0241+622 at short baseline was at most several degrees and does not show systematic variation due to the diurnal motion. On the other hand, it is clear that the closure phase at long baseline varied thus showing the effect of structure at long baseline. The variation was up to 50 degrees which was consistent with above phase delay estimation. Since, the structure effect in closure phase was seen only long baseline ($\geq$ 5000 km) with up to 50 degrees, the results are consistent with $\leq$ 75 μas in angular size in the sky.

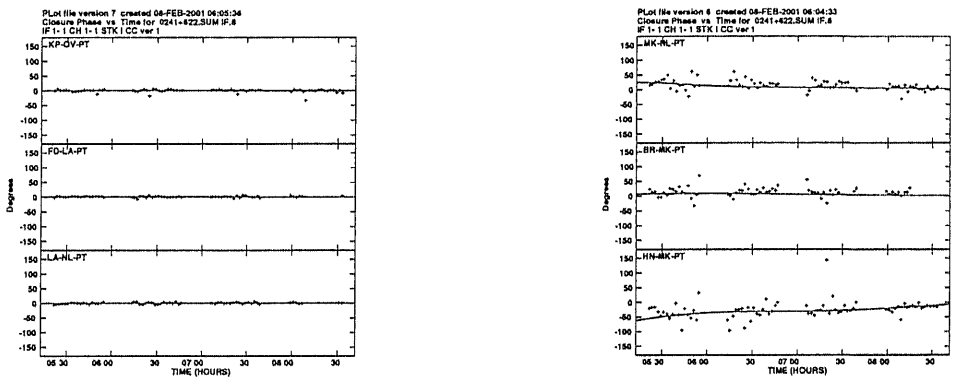

Figure 6.2: Closure phase of ICRF0241+622. Left figure shows the short baseline case. Right figure shows the long baseline case. The structure effect is evident at long baseline.

6.3.3 Estimated total error for each observation

Estimated total errors for each observation are shown in Table 6.7, 6.8 and 6.9. Reference source structure effect and baseline length error were translated to angular size in the sky at 4000 km baseline. The accuracies of each observation were reached about 100 μas at 4000 km baseline.

	ΔRight Ascension (μ as)	ΔDeclination (μ as)
July 1998		
ICRF2100+468 statistical Gaussian fitting error	3	5
ICRF2100+468 structure effect	97	97
IRAS21008+4700 statistical Gaussian fitting error	12	23
Baseline length error	1	1
Root-Square-Sum	98	100
August 1998		
ICRF2100+468 statistical Gaussian fitting error	5	9
ICRF2100+468 structure effect	85	85
IRAS21008+4700 statistical Gaussian fitting error	14	24
Baseline length error	1	1
Root-Square-Sum	86	89

Table 6.7: Error estimations of IRAS21008+4700 -36.56 km/s feature

	ΔRight Ascension (μ as)	ΔDeclination (μ as)
July 1998		
ICRF2100+468 statistical Gaussian fitting error	3	5
ICRF2100+468 structure effect	97	97
IRAS21008+4700 statistical Gaussian fitting error	16	30
Baseline length error	1	1
Root-Square-Sum	98	102
August 1998		
ICRF2100+468 statistical Gaussian fitting error	5	9
ICRF2100+468 structure effect	85	85
IRAS21008+4700 statistical Gaussian fitting error	40	77
Baseline length error	1	1
Root-Square-Sum	94	115

Table 6.8: Error estimations of IRAS21008+4700 -71.21 km/s feature

	ΔRight Ascension (μ as)	ΔDeclination (μ as)
November 1999		
ICRF0241+622 statistical Gaussian fitting error	15	24
ICRF0241+622 structure effect	93	93
W3(OH) statistical Gaussian fitting error(median)	13	21
Baseline length error	16	16
Root-Square-Sum	96	100
December 1999		
ICRF0241+622 statistical Gaussian fitting error	15	33
ICRF0241+622 structure effect	92	92
W3(OH) statistical Gaussian fitting error(median)	13	33
Baseline length error	16	16
Root-Square-Sum	94	104

Table 6.9: Error estimations of median maser spots in W3(OH)

Chapter 7

Discussion

7.1 Possibility of detection of outer Galactic rotation

7.1.1 Comparison of the results on IRAS21008+4700 – ICRF2100+468 pair with Galactic rotation model

We compared the above results with model predictions. We assumed a simple flat Galactic rotation model with the Galactic center distance of 8.5 kpc and rotation speed near the Sun of 220 km/s. We also take into consideration the annual parallax and Solar motion. For the Solar motion, the speed of 19.5 km/s and solar apex direction $\alpha = 271°$ and $\delta = +29°$ are adopted. The results are shown in Figure 7.1.1.

In general, proper motions of Galactic source relative to extragalactic source are due to annual parallax, Galactic rotation, Solar motion and intrinsic motion of the Galactic source itself. The intrinsic motion of IRAS21008+4700 is likely to be small since a simple flat rotation model of the Galaxy predicts a kinematic distance of 7.3 kpc for IRAS21008+4700 with central LSR velocity of -50 km/s.

The annual parallax and Solar motion also may be small because of the same reason. However, the Galactic rotation is larger than other effects according to the flat rotation model. IRAS21008+4700 is located in $l =$

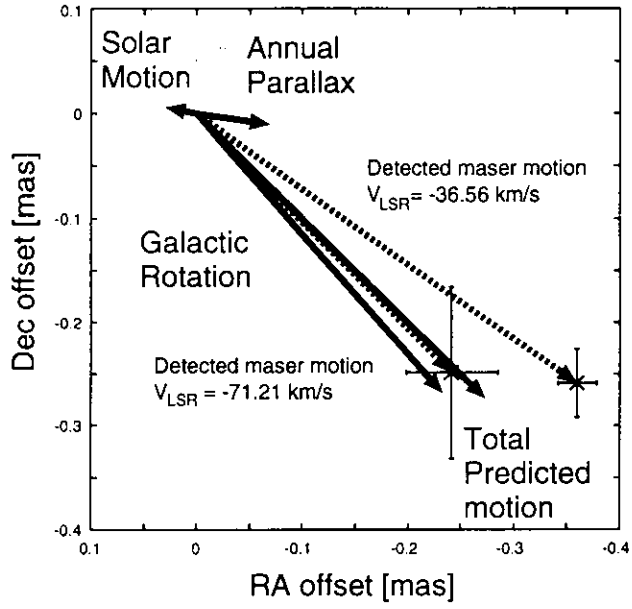

Figure 7.1: Comparison of our VLBA results with values predicted from the flat rotation model of the Galaxy. Dashed line are the detected proper motions with statistical error for each feature in IRAS21008+400.

88.1°. This direction is nearly equal to the direction of the Galactic rotation near the Sun. Therefore, the apparent proper motion is mostly due to the Galactic rotation of the maser source.

We conclude that we detected real displacements of the maser features in IRAS21008+4700 during a month because :

1. The observed displacements are around 400 μas and much larger than the statistical error of several tens μas and the estimated total error of 100 μas.

2. They are along the Galactic plane in the right direction of the Galactic rotation.

3. They are in good agreement with the expected motion due mostly to the Galactic rotation along with smaller contributions from annual parallax and Solar motion of the maser source.

This consistency strongly suggests that ICRF2100+468 is an extragalactic source. However, it is necessary to measure redshift of this source or proper motion itself relative to known extragalactic source to definitely answer whether ICRF2100+468 is extragalactic or not.

7.1.2 Results on W3(OH) – ICRF0241+622 and distance to W3(OH)

On the other hand, detected proper motions of W3(OH) maser features were mostly in North East - South West direction. The direction is not parallel to the Galactic plane unlike in the case of IRAS21008+4700. Since W3(OH) is much nearer from the Sun than IRAS21008+4700, annual parallax and Solar motion are larger than in the case of IRAS21008+4700. Therefore, disagreement between Galactic plane and the direction of detected proper motions is caused by the effects of annual parallax and Solar motion. We show the expected displacements due to the three effects and the median of the observed displacements of the maser features assuming the distance 2.3 kpc (Figure 7.1.2).

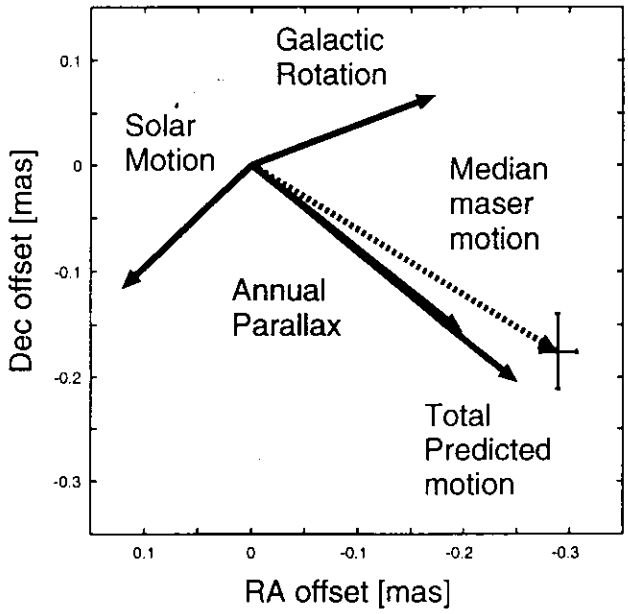

Figure 7.2: Comparison of our VLBA results with values predicted from the flat rotation model of the Galaxy. Dashed line is the detected average proper motion with statistical error. Distance of W3(OH) is assumed to be 2.3 kpc.

However, distance to W3(OH) is not well known. Georgelin and Georgelin (1976) estimated the distance to IC1848 (S199) in W3 region to be 2.3 kpc based on their rotation curve, older Galactic constant R_0 = 10 kpc and Θ_0 = 250 km/s and LSR velocity of the HII region -36.6 km/s. Palagi et al. (1993) in thier survey of water maser sources gave 4.97 kpc as estimated distance to W3(OH). Our estimation of the statistical parallax in Chapter 5 yielded the value 3.33 kpc for the distance. Moreover, if we assume that the LSR velocity of -36.6 km/s of IC1848 is due to the Galactic rotation, the simple flat rotation model described in the previous section predicts kinematic distance of 3.31 kpc.

It is interesting to compare the median of the observed displacements with predictions of the flat rotation model with three different distance values. Figures 7.3, 7.4 and 7.5 show the predicted motion and observed motion for three different values of the distance : 2.3 kpc, 3.31 kpc and 4.97 kpc.

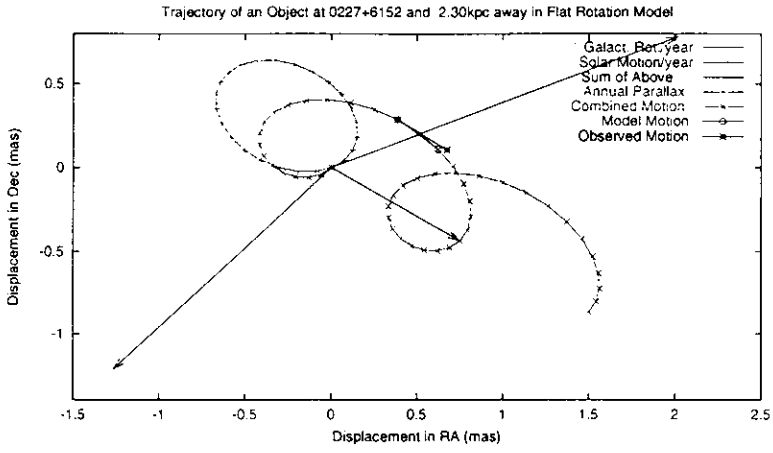

Figure 7.3: Expected proper motion of W3(OH) relative to adjacent extragalactic source ICRF0241+622. The distance to W3(OH) of 2.30 kpc was assumed.

The figures show that the prediction based on distance values of 2.3 kpc and 3.31 kpc are roughly consistent with the observed motion. However, if we adopt 4.97 kpc, discrepancy between the model and observation is

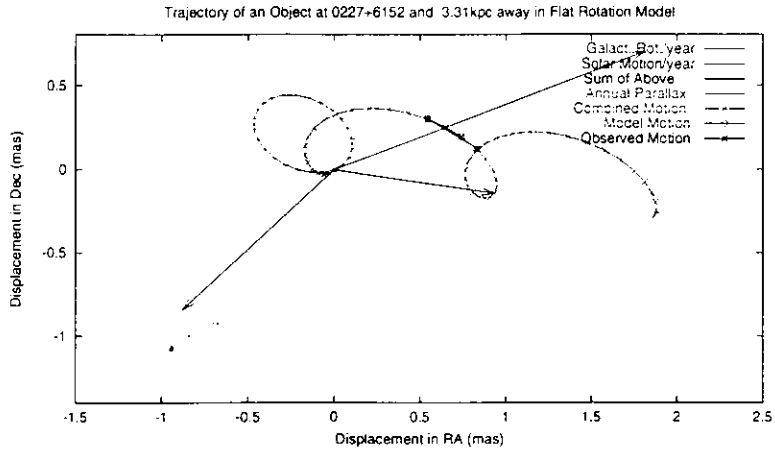

Figure 7.4: Expected proper motion of W3(OH) relative to adjacent extragalactic source ICRF0241+622. The distance to W3(OH) of 3.31 kpc was assumed.

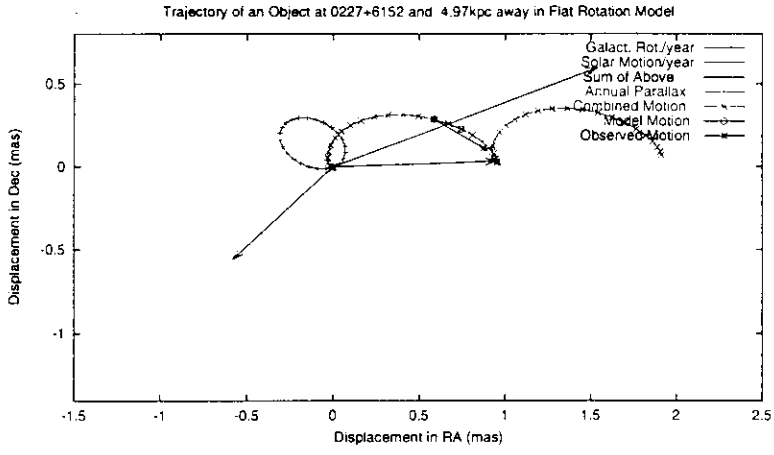

Figure 7.5: Expected proper motion of W3(OH) relative to adjacent extragalactic source ICRF0241+622. The distance to W3(OH) of 4.97 kpc was assumed.

rather large. Therefore, we are inclined to prefer the nearer distance of W3(OH). It dose not seem very productive however to attempt to estimate the distance of W3(OH) based on the present results only, in view of the possible large systematic errors and uncertainties of the Galactic model. It seems much more promising to directly determine the trigonometric parallax of W3(OH). The figure 7.1.2, 7.3, 7.4 and 7.5 clearly show that the parallax will be well measured if we achieve the positional accuracy of a few tens microarc-second.

7.1.3 Towards kilo persec scale astrometry

The statistical error of the present phase-referencing VLBI at 22 GHz was as small as a few to several tens microarc-second. The estimation of the uncorrected systematic errors showed the total accuracy of 100 μas. With this accuracy, one can determine the annual parallax of an object at D kpc with 10 $\times$ D persent accuracy and physical velocity perpendicular to the line of sight at D kpc with 0.5 $\times$ D km/s accuracy. The accuracy is already adequate for study of the non-circular motion of the Galaxy which is expected to have the magnitude of 10 km/s.

Therefore, phase-referencing VLBI at 22 GHz can be carried out beyond HIPPARCOS accuracy. However, the accuracy of the present results was estimated in single epoch. If reference source structure is stable during mutli-epoch observations and observed in the same uv coverage, the phase error due to reference source structure and baseline error may be canceled by comparing observations at different epochs. Then, the accuracy of phase-referencing VLBI will be better than the present results. That is, it is possible to observe between target and reference sources with 10 μas accuracy. The 10μas accuracy can be carried out astrometry throughout whole of the Galaxy and detection of proper motions of local group of galaxies.

Therefore, the present observations is the first step of kilo persec scale astrometry.

In addition, our proposal for multi-epoch observations (7 times during a year) of IRAS21008+4700 and ICRF2100+468 pair and W3(OH) and

ICRF0241+622 pair was accepted by VLBA. Main aim of this project is detection of annual parallax. First epoch and second epoch observation of IRAS pair was carried out in September 2000. (See Figure 9.1)

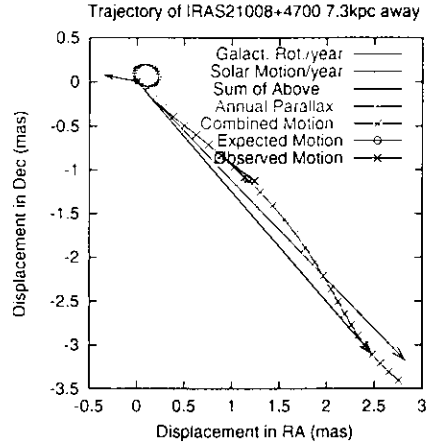

Figure 7.6: Expected proper motion of IRAS2100+4700 relative to adjacent extragalactic source ICRF2100+468

Chapter 8

Conclusion

New results obtained in the present study are the followings.

1. We succeeded for the first time in fast-switching phase-referencing VLBI observations between water maser and continuum sources at 22 GHz. In fact, we successfully derived very smooth time series of the fringe-phase-difference observables and estimated relative positions for two pairs of maser and continuum sources IRAS21008+4700-ICRF2100+468 and W3(OH)-ICRF0241+622.

2. We demonstrated for W3(OH)-ICRF0241+622 pair that the atmospheric phase fluctuation effect is well compensated in the phase difference observable. In fact, the upper limit of the residual atmospheric fluctuation effect in the 40-second-averaged differential phase is estimated to be as small as 10 degrees which corresponds to 37 μas for a 2000 km projected baseline at 22 GHz.

3. We detected displacements of water maser sources several kiloparsecs away with respect to adjacent reference continuum sources from two observations separated by a month. The observed displacement for IRAS21008+4700-ICRF2100+468 pair was around 400 μas with position angle of about 130 degree, while the displacement for W3(OH)-ICRF0241+622 pair was around 338 μas with position angle of about

121 degree. These displacements are in general agreement with vector sums of predicted displacements due to the Galactic rotation, annual parallax and Solar motion.

4. Statistical errors in the measured displacements of individual features in the maser sources estimated by the one Gaussian component fit range from 7 μas to 232 μas with median value of 25 μas for W3(OH)-ICRF0241+622 pair, and 70 μas and 20 μas for the two features of IRAS21008+4700-ICRF2100+468 pair. On the other hand, systematic errors, reference source structure effect and baseline error, were estimated to be about 100 μas.

On the basis of the above results, we conclude that the phase-referencing VLBI is able to realize the high-precision astrometry of Galactic water maser sources with 10 μas level accuracy and to detect annual parallaxes and proper motions of maser sources in kiloparsec scale.

Acknowledgment

First of all, I would like to take this opportunity to thank to my supervisor Prof. Tetsuo Sasao. Also I would like to thank the Drs. Satoko-Sawada-Sato, Makoto Miyoshi, Hiroshi Imai, Mareki Honma, VERA project and Japan VLBI network members with suggestions of observation schedules, data reductions and interpretations of results. In VLBA observations, I would like to thank Dr. Vivek Dhawan, whose contribution for our projects were very helpful.

Finally, I would like to thank my parents and my brothers.

Bibliography

[1] ALCOLEA, J., K.M.MENTEN, J.M.MORAN, & M.J.REID 1992, The proper motions of the H_2O masers near W3(OH)., *Astronomical Masers*, 225

[2] ARGON, A.L., GREENHILL, L.J., MORAN, J.M., REID, M.J., & MENTEN, K.M 1998, *Radio Emission from Galactic and Extragalactic Compact Sources*, ASP Conf. Series, Vol 144, IAU Colloquium 164, eds. J.A. Zensus, G.B. Taylor, & J.M. Wrobel, p.235.

[3] Y.ASAKI, M.SAITO, R.KAWABE, K.MORITA, & T.SASAO 1996 Phase Compensation Experiments Using the Paired Antennas Method, Radio Science, 6, 1615

[4] BARTEL, N., HERRING, T.A., RATNER, M.I., SHAPIRO, I.I., & COREY, B.E. 1986, VLBI limits on the proper motion of the 'core' of the superluminal quasar 3C345, Nature, 319, 733

[5] BEASLEY, A.J., & CONWAY, J.E. 1995, in ASP Conf.Ser.82, *Very Long Baseline Interferometry and the VLBA*, eds. J.A.Zensus, P.J.Diamond, & P.J.Napier (San Francisco: ASP), 327

[6] BENEDICT, G.F., MCARTHUR, B.E., FRANZ, O.G., WASSERMAN, L.H., & HENRY, T.J. 2000, Interferometric Astrometry of the Low-Mass Binary GL 791.2 (= HU Del) Using Hubble Space Telescope Fine Guidance Sensor 3: Parallax and Component Masses, AJ,120,1106

[7] A.H.Bridle & E.W.Greisen 1994, The NRAO AIPS Project - A Summary, AIPS Memo, 51

[8] T.V.Cawthorne, J.M.Moran, & M.J.Reid 1992, Preliminary results from a study of the proper motion of water vapor masers in Cepheus A., *Astronomical Masers*, 237

[9] Counselman, C.C., III, Kent, S.M., Knight, C.A., Shapiro, I.I., Clark, T.A., Hinteregger, H.F., Rogers, A.E.E., & Whitney, A.R. 1974, Solar Gravitational Deflection of Radio Waves Measured by Very Long Baseline Interferometry, Phys. Rev. Lett., 33, 1621

[10] Desmurs, J. F., Bujarrabal, V., Colomer, F.,& Alcolea, J. 2000, LBA observations of SiO masers: arguments in favor of radiative pumping mechanisms, A & A ,360, 189

[11] N.Duric, P.C.Gregory, & A.R.Taylor 1987, Two-epoch VLA observations of variable Galactic plane radio sources, AJ, 93, 890

[12] J.H.Elias, K.Matthews, G.Neugebauer, & B.T.Soifer 1985, A 2.2-μm search for variable Galactic plane radio sources, AJ, 90, 1188

[13] Elitzur M. 1992 *Astronomical Masers*, Kluwer Academic Publishers, Dordrecht

[14] Feast, M. W., & Catchpole, R. M. 1997, The Cepheid period-luminosity zero-point from HIPPARCOS trigonometrical parallaxes, MNRAS,286L,1

[15] Fomalont, E. B., Goss, W. M., Beasley, A. J., & Chatterjee, S. 1999, Sub-Milliarcsecond Precision of Pulsar Motions: Using In-Beam Calibrators with the VLBA, AJ,117,3025

[16] Fricke, W. 1975, Determination of a new Fundamental Reference Coordinate System (FK5) for Astronomy, Bull. American Astron. Soc., 7, 339

[17] GENZEL,R., REID,M.J., MORAN,J.M., & DOWNES,D. 1981a, Proper motions and distances of H2O maser sources I - The outflow in Orion-KL, ApJ, 244, 884

[18] GENZEL,R., DOWNES,D., SCHNEPS,M.H., REID,M.J., MORAN,J.M., KOGAN,L.R., KOSTENKO,V.I., MATVEENKO,L.I., & RONNANG,B. 1981b, Proper motions and distances of H2O maser sources. II - W51 MAIN, ApJ, 247, 1039

[19] GENZEL, R., PICHON, C., ECKART, A., GERHARD, O.E., & OTT, T. 2000, Stellar dynamics in the Galactic Centre: proper motions and anisotropy, MNRAS,317,348

[20] GEORGELIN, Y.M., & GEORGELIN, Y.P. 1976, The spiral structure of our Galaxy determined from HII regions., A & A, 49, 57

[21] Greenhill, L.J., Moran, J.M., Reid, M.J., Menten, K.M., & Hirabayashi,H. 1993, Microarcsecond proper motions of extragalactic water vapor masers in M33, ApJ,406,482

[22] P.C. GREGORY, & A.R.TAYLOR 1981, Radio Patrol of the Northern Milky Way : A Survey for Variable Sources, ApJ, 248,596

[23] J.C.GUIRADO, J.M.MARCAIDE, M.A.PÉRES-TORRES, & E.ROS 2000, VLBI difference astrometry at 43 GHz, A & A, 353, L37

[24] GWINN, C. R., TAYLOR, J. H., WEISBERG, J. M., & RAWLEY, L. A. 1986, Measurement of pulsar parallaxes by VLBI,AJ,91,338

[25] GWINN, C. R., MORAN, J.M., & REID, M.J 1992, Distance and kinematics of the W49N H2O maser outflow, ApJ, 393, 149

[26] GWINN, C. R. 1994, Hypersonic acceleration and turbulence of H_2O masers in W49N,ApJ,429,241

[27] HERRNSTEIN, J.R. 1997, Observations of the Sub-Parsec Maser Disk in NGC4258, Ph.D thesis, Harvard Univ.

[28] HEWITT, A. AND BURBIDGE, G. 1987, A new Optical catalog of quasi-stellar objects, ApJS, 63, 1

[29] HIRABAYASHI.H, ET AL 2000, The VLBI Space Observatory Programme and the Radio-Astronomical Satellite HALCA, PASJ, 52, 995

[30] HONMA, M., *et al* 2000a, J-Net Galactic -Plane Survey of VLBI Radio Sources for VLBI Exploration of Radio Astrometry (VERA), PASJ, 52, 631

[31] HONMA, M., 2000b, Science with VERA : VLBI Exploration of Radio Astrometry. *Proceedings of SPIE*, **4015**, 624

[32] HORNER,S.D., GERMAIN,M.E., GREENE,T.P., JOHNSTON,K.J., MONET,D.G., MURISON,M.A., PHILLIPS,J.D., REASENBERG,R.D., SEIDELMANN,P.K., & URBAN,S.E. 1998, FAME - The Full-sky Astrometric Mapping Explorer, AAS, 193, 1206

[33] H.IMAI 1999, Internal motions and fine structure of Astronomical Masers, Ph.D. Thesis.

[34] H.IMAI, O.KAMEYA, T.SASAO, M.MIYOSHI, S.DEGUCHI, S.HORIUCHI & Y.ASAKI 2000, Kinematics and distance of water masers in W3 IRS 5, ApJ, 538,751

[35] JOHNSTON, K.J.,JOHNSTON, K. J., FEY, A. L., ZACHARIAS, N., RUSSELL, J. L., MA, C., DE VEGT, C., REYNOLDS, J. E., JAUNCEY, D. L., ARCHINAL, B. A., CARTER, M. S., CORBIN, T. E., EUBANKS, T. M., FLORKOWSKI, D. R., HALL, D. M., MCCARTHY, D. D., MCCULLOCH, P. M., KING, E. A., NICOLSON, G.,& SHAFFER, D. B. 1995, A radio reference frame. ApJ, 110, 880

[36] VAN LANGEVELDE, H. J., VLEMMINGS, W., DIAMOND, P. J., BAUDRY, A., & BEASLEY, A. J. 2000, VLBI astrometry of the stellar image of U Herculis, amplified by the 1667 MHz OH maser, A & A,357,945

[37] Lestrade,J.-F., Jones,D.L., Preston, R. A., Phillips, R. B., Titus, M. A., Kovalevsky, J., Lindegren, L., Hering, R., Froeschle, M., Falin, J. L., Mignard, F., Jacobs, C. S., Sovers, O. J., Eubanks, M., & Gabuzda, D. 1995, Preliminary link of the HIPPARCOS and VLBI reference frames A & A, 304, 182

[38] LESTRADE, J.-F, PRESTON, R. A., JONES, D. L., PHILLIPS, R. B., ROGERS, A. E. E., TITUS, M. A., RIOJA, M. J., & GABUZDA, D. C. 1999, High-precision VLBI astrometry of radio-emitting stars. A & A, 344, 1014

[39] LINDEGREN, L., & PERRYMAN, M. A. C. 1996, GAIA: Global astrometric interferometer for astrophysics ,A & AS, 116, 579

[40] MARCAIDE, J.M., & SHAPIRO, I.I. 1983, High Precision Astrometry via Very-Long Baseline Radio Interferometry: Estimate of the Angular Sepa ration between the Quasars 1038+528A and B, AJ, 88, 1133- 1137.

[41] MARCAIDE, J.M., ELOSEGUI, P., & SHAPIRO, I.I. 1994, On the Relative Proper Motion of Quasars 1038+528 A,B., AJ, 108, 368

[42] 1996, The Circumstellar Environment of Evolved Starsas Revealed by Studies of Circumstellar Water Masers, Ph.D. thesis, New Mexico State Univ.

[43] MIYOSHI, M., MATSUMOTO, K., KAMENO, S., TAKABA, H., & IWATA, T. 1994, Collisional Pumping of SIO Masers in Evolved Stars, Nature,371,395

[44] MIYOSHI, M., MORAN, J., HERRNSTEIN, J., GREENHILL, L., NAKAI, N., DIAMOND, P.,& INOUE, M. 1995, Evidence for a Black-Hole from High Rotation Velocities in a Sub-Parsec Region of NGC4258, Nature, 373,127

[45] J.M. MORAN 1989, *Very Long Baseline Interferometry Techniques and Applications*, 47

[46] P.J.NAPIER 1995, in ASP Conf.Ser.82, *Very Long Baseline Interferometry and the VLBA*, eds. J.A.Zensus, P.J.Diamond, & P.J.Napier (San Francisco: ASP), 59

[47] A.J.NORTON, M.J.COE, S.J.UNGER, B.MARGON, & A.C.PHILLIPS 1993, Infrared observations of highly variable radio sources in the galactic plane, MNRAS, 260,883

[48] OMODAKA T., MORIMOTO M., ET AL 1994, in: VLBI TECHNOLOGY, Progreee and Future Observational Possibilities, eds. T.Sasao, S.Manabe, O.Kameya, M.Inoue, Terra Scientific Publishing Company, Tokyo, 191

[49] F.PALAGI., ET AL. 1993, Classification and statistical properties of galactic H_2O masers, A & AS, 101, 153

[50] PALUMBO, G. G. C., SCAPPINI, F., PARESCHI, G., CODELLA, C., CASELLI, P.,& ATTOLINI, M. R. 1994, IRAS-selected Galactic star-forming regions - I. New $6_{16} \rightarrow 5_{23}$ water maser detections in molecular cores north of Dec.+15°., MNRAS,266, 123

[51] M.A.PÉREZ-TORRES, J.M.MARCAIDE, J.C.GUIRADO, E.ROS, I.I.SHAPIRO, M.I.RATNER, & E.SARDÓN 2000, Towards global phase-delay VLBI astrometry: observations of QSO1150+812 and BL1803+784, A & A, 360, 161

[52] PERRYMAN, M. A. C., LINDEGREN, L., KOVALEVSKY, J., TURON, C., HOEG, E. , GRENON, M., SCHRIJVER, H., BERNACCA, P. L., CREZE, M., DONATI, F., EVANS, D. W., FALIN, J. L., FROESCHLE, M., GOMEZ, A., GREWING, M., VAN LEEUWEN, F., VAN DER MAREL, H., MIGNARD, F., MURRAY, C. A., PENSTON, M. J., PETERSEN, C., LE POOLE, R. S., WALTER, H. G., 1995, Parallaxes and the Hertzsprung-Russell diagram for the preliminary HIPPARCOS solution H30, A & A, 304, 69

[53] PERRYMAN, M. A. C., BROWN, A. G. A., LEBRETON, Y., GOMEZ, A., TURON, C., DE STROBEL, G. CAYREL, MERMILLIOD, J. C., ROBICHON, N., KOVALEVSKY, J., CRIFO, F., 1998, The Hyades: distance, structure, dynamics, and age, A & A, 331, 81

[54] REID, M.J., SCHNEPS, M.H., MORAN, J.M., GWINN, C.R., GENZEL, R., DOWNES, D., & ROENNAENG, B. 1988a, The distance to the center of the Galaxy - H2O maser proper motions in Sagittarius B2(N), ApJ, 330, 817

[55] REID, M.J., GWINN, C.R., MORAN, J.M., GWINN, C.R., & MATTHEWS, A.H. 1988b, R_0 from H2O maser proper motions in SGR B2-middle, BAAS, 20, 1017

[56] REID, M. J., & MORAN, J.M. 1988, in *Galactic and Extragalctic Radio Astronomy*, eds. G.L.Verschuur and K.I.Kellermann, 2nd Edition, 255

[57] Reid, M. J., Readhead, A. C. S., Vermeulen, R. C., & Treuhaft, R. N. 1999, The Proper Motion of Sagittarius A*. I. First VLBA Results, ApJ,524,816

[58] RIOJA, M. J., STEVENS, E., GURVITS, L., ALEF, W., SCHILIZZI, R. T., SASAO, T., & ASAKI, Y. 1997, Phase-referencing in cluster-cluster VLBI mode., Vistas in Astronomy,41,213

[59] ROS, E., MARCAIDE, J. M., GUIRADO, J. C., RATNER, M. I., SHAPIRO, I. I., KRICHBAUM, T. P., WITZEL, A., & PRESTON, R. A. 1999, High precision difference astrometry applied to the triplet of S5 radio sources B1803+784/Q1928+738/B2007+777, A & A, 348,381

[60] S.ROSER, U.BASTIAN, K.S.DE BOER, E.HOG, H.P.ROSER, C.SCHALINSKI, E.SCHILIBACH, CH.DEVEGT, & S.WAGNER 1997, in: Hipparcos Venice '97, 777

[61] T.SASAO 1997, Investigation of the interferometer phase compensation method on VERA project, *in Japanese*, Proceedings of Japanese VLBI Network Colloquium, 111

[62] S. SAWADA-SATOH, M.INOUE, K.M.SHIBATA, S.KAMENO, V.MIGENES, N.NAKAI, & P.J.DIAMOND 2000, The Nuclear Region of the Seyfert 2 Galaxy NGC3079, PASJ,52,421

[63] SCHILIZZI, R. T. 1995, in ASP Conf.Ser.82, *Very Long Baseline Interferometry and the VLBA*, eds. J.A.Zensus, P.J.Diamond, & P.J.Napier (San Francisco: ASP), 59

[64] SCHNEPS,M.H., MORAN,J.M., GENZEL,R., REID,M.J., LANE,A.P., & DOWNES,D. 1981, Proper motions and distances of H2O maser sources. III - W51 NORTH, ApJ, 249, 124

[65] SHAFFER, D.B. 1995, in ASP Conf.Ser.82, *Very Long Baseline Interferometry and the VLBA*, eds. J.A.Zensus, P.J.Diamond, & P.J.Napier (San Francisco: ASP), 345

[66] SHAO, MICHAEL, 1998, SIM: the space interferometry mission SPIE, 3350, 536.

[67] SJOUWERMAN, LORANT O., VAN LANGEVELDE, HUIB JAN, DIAMOND, PHILIP J. 1998, Stellar positions from SiO masers in the Galactic center, *A & A*,339, 897

[68] Y.SOFUE, & V.RUBIN 2100, Rotation Curves of Spiral Galaxies, Ann.Rev.Astron. & Astrophys., Vol 39

[69] A.R.TAYLOR, & E.R. SEAQUIST 1984, HI absorption in the direction of Galactic-plane variables: Evidence for new, rapidly variable extragalactic radio sources, AJ, 89,1692

[70] THOMPSON, A.R., MORAN, J.M., SWENSON, G.W., 1986, *Interferometry and Synthesis in Radio Astronomy*, John Wiley

[71] T.TSUJIMOTO, M.MIYAMOTO, & Y.YOSHII 1998, The absolute magnitude of RR Lyrae stars derived from the *Hipparcos* Catalogue, ApJ, 492, L79

[72] TZIOUMIS, A. K. 1997, The Australian LBA-status and developments, *Vistas in Astronomy*, 41, 311

[73] J.S.ULVESTAD 1999, in ASP Conf.Ser.180, *Synthesis Imaging in Radio Astronomy II*, eds. G.B.Taylor, C.L.Carilli, & R.A.Perley (San Francisco: ASP), 513

[74] WEINREB S., MEEKS M.L., CARTER J.C., BARRETT A.H., & ROGERS A.E.E. 1965, Nature, 208,440